Acta Geotechnica (2022) 17:1477–1502
https://doi.org/10.1007/s11440-021-01440-1

RESEARCH PAPER

Comparative performance of eight ensemble learning approaches for the development of models of slope stability prediction

Shan Lin[1,2] · Hong Zheng[1] · Bei Han[1] · Yanyan Li[1] · Chao Han[1] · Wei Li[3]

Received: 19 February 2021 / Accepted: 4 December 2021 / Published online: 23 January 2022

Abstract

Slope engineering is a complex nonlinear system. It is difficult to respond with a high level of precision and efficiency requirements for stability assessment using conventional theoretical analysis and numerical computation. An ensemble learning algorithm for solving highly nonlinear problems is introduced in this paper to study the stability of 444 slope cases. Different ensemble learning methods [AdaBoost, gradient boosting machine (GBM), bagging, extra trees (ET), random forest (RF), hist gradient boosting, voting and stacking] for slope stability assessment are studied and compared to make the best use of the large variety of existing statistical and ensemble learning methods collected. Six potential relevant indicators, γ, C, φ, β, H and r_u, are chosen as the prediction indicators. The tenfold CV method is used to improve the generalization ability of the classification models. By analysing the evaluation indicators AUC, accuracy, kappa value and log loss, the stacking model shows the best performance with the highest AUC (0.9452), accuracy (84.74%), kappa value (0.6910) and lowest log loss (0.3282), followed by ET, RF, GBM and bagging models. The analysis of engineering examples shows that the ensemble learning algorithm can deal with this relationship well and give accurate and reliable prediction results, which has good applicability for slope stability evaluation. Additionally, geotechnical material variables are found to be the most influential variables for slope stability prediction.

Keywords Classification · Ensemble learning · Machine learning (ML) · Repeated cross-validation · Slope stability

1 Introduction

Due to the needs of economic development and the expansion of the scope of geotechnical engineering, as an essential environment for human survival, slopes are a crucial part of engineering construction, and research on their stability is constantly developing and advancing.

Slope stability evaluation is a crucial research aspect in slope engineering. However, the slope deformation and failure process is a very complex geological process. The factors that affect the slope stability are uncertain [27], so it is not easy to accurately evaluate slope stability with traditional theoretical analysis [13] and numerical calculations (such as the finite element method [20], discontinuous deformation analysis [60, 61, 70], virtual element method [33, 48] and phase-field [65–67]). Slope engineering is an uncertain, nonlinear, dynamic and open complex system. Its stability is comprehensively affected by geological and engineering factors with randomness, fuzziness, variability and other uncertain characteristics. There is a highly nonlinear relationship between slope stability and influencing factors. Therefore, the inevitable slope stability research trend is to break through traditional deterministic thoughts and fully consider the uncertainty caused by various slope factors. Slope stability analysis can be regarded as a pattern recognition task [59]. Based on the slope information database [51], some scholars use machine learning (ML) [35, 38, 50] to judge slope stability. Lu et al. [36] used an artificial neural network (ANN) [2] to predict the failure of

✉ Bei Han
hanbxie@bjut.edu.cn

[1] Key Laboratory of Urban Security and Disaster Engineering of China Ministry of Education, Beijing University of Technology, Beijing 100124, China

[2] State Key Laboratory of Geomechanics and Geotechnical Engineering, Institute of Rock and Soil Mechanics, Chinese Academy of Sciences, Wuhan 430071, China

[3] School of Civil Engineering and Architecture, Linyi University, Linyi 276000, China

circular slopes, which showed that the ANN has obvious advantages compared with the maximum likelihood estimation (MLE) technique. Samui [44] studied the application of a support vector machine (SVM) to predict slope stability. Sakellariou et al. [43] established a series of ANNs to predict the safety factor of the slope wedge failure mechanism and circular failure mechanism and evaluate their stability. Dickson et al. [9] introduced three ML algorithms to analyse the control of coastal cliff landslides. Yan et al. [57] studied the application of the Bayes discriminant analysis method in the stability prediction of open pit slopes. Zhou et al. [63] introduced six supervised learning methods to predict the stability of hard rock pillars, and the performance of these algorithms was compared and analysed. Cheng and Hoang [8] used a novel bee colony optimized support vector classifier to evaluate the slope collapse caused by a typhoon. Lee et al. [29] and Lin et al. [32] established a slope stability prediction model using an ANN. Based on ML, Hoang et al. [23] used the least squares support vector classification (LS-SVC) and firefly algorithm (FA) methods to study 168 slope cases. All the above artificial intelligence models can help us better understand the slope status, but each model has advantages and disadvantages. Due to the complexity of the problem, there are still some imperfections in these methods. Different algorithms have different sensitivities to the same type of data, and the classification accuracy of the same category under different algorithms will also vary. Each classifier has its limitations. The focus of slope stability evaluation research is the ML algorithm, which constantly looks for newer and more robust ML algorithms to establish slope stability evaluation models to achieve better prediction results. Therefore, it is necessary to find intelligent algorithms with high accuracy and strong applicability. Ensemble learning trains multiple algorithms to achieve complementary advantages and obtain better slope stability prediction results than the single algorithm.

Ensemble learning forms a more comprehensive 'strong learner' through the combination of multiple models. Ensemble learning can obtain more accurate prediction results, with better generalization performance and broader applications [10, 11]. Ensemble learning has been successfully applied to character recognition [12], medical diagnosis [62], facial recognition [21] and seismic wave classification [46]. Lin et al. [34] applied four supervised learning algorithms (random forest (RF), gravitational search algorithm (GSA), SVM and naive Bayesian) to slope stability evaluation. They carried out a comparative analysis to prove that the performance of RF and GSA is better than other algorithms. Based on an updated database of case histories, Zhou et al. [64] proposed a prediction method for slope stability analysis using the gradient boosting machine (GBM) method. Qi and Tang [42] used FA to adjust the superparameters and verified and discussed the feasibility of six comprehensive methods (logistic regression (LR), RF, decision trees (DT), GBM, multilayer perceptron neural network and SVM) in slope stability prediction. Qi and Tang [41] proposed a slope stability evaluation algorithm, adaptive boosted decision trees (ABDT), quadratic discriminant analysis (QDA), SVM, ANN, Gaussian process classification (GPC) and K-nearest neighbours (KNN) as individual classifiers and a weighted majority voting method as the combined classifier. The results show that the hybrid ensemble method greatly improves slope stability prediction performance. Previous studies have shown that ensemble learning can provide a feasible tool for constructing a slope stability discrimination system, which allows the classification of slope stability. However, there is no comprehensive comparison of classifier ensemble algorithms over the prediction of slope stability. To improve the prediction accuracy of nonlinear slope behaviour and establish a simple model that can be widely promoted, it is necessary to continue exploring an ensemble algorithm that is more suitable for analysing nonlinear slope behaviour.

Because of this, the primary purpose of this paper is to compare the applicability of different classifier ensemble algorithms in slope stability analysis. To achieve this goal, we developed a research method for comparing the performance of different classifier ensemble algorithms in Scikit-learn [40], including bagging, RF, AdaBoost, GBM, stacking, voting and extra trees (ET) and hist gradient boosting classifier (HGB). These ensemble learning algorithms are specifically selected because they are increasingly used in engineering, but they have not been thoroughly compared with each other. In Sect. 2, the ensemble learning algorithm is briefly introduced, and Sect. 3 analyses the slope dataset. In Sect. 4, these methods are applied to classify slope stability, and the results are discussed according to performance criteria. The conclusion of this study is presented in the final section.

2 Ensemble learning methods

Ensemble learning [10] is a process of effective fusion to form a strong classifier based on individual learners (as shown in Fig. 1). According to the difference of the combination methods of base learners, ensemble learning can be divided into parallel topology structure (representing algorithm is bagging), serial topology structure (representing algorithm is boosting) and hybrid topology structure (representing algorithm is stacking). In this study, we consider several common ensemble learning algorithms in Scikit-learn. All these methods are increasingly being used and have efficient implementations; some of these methods

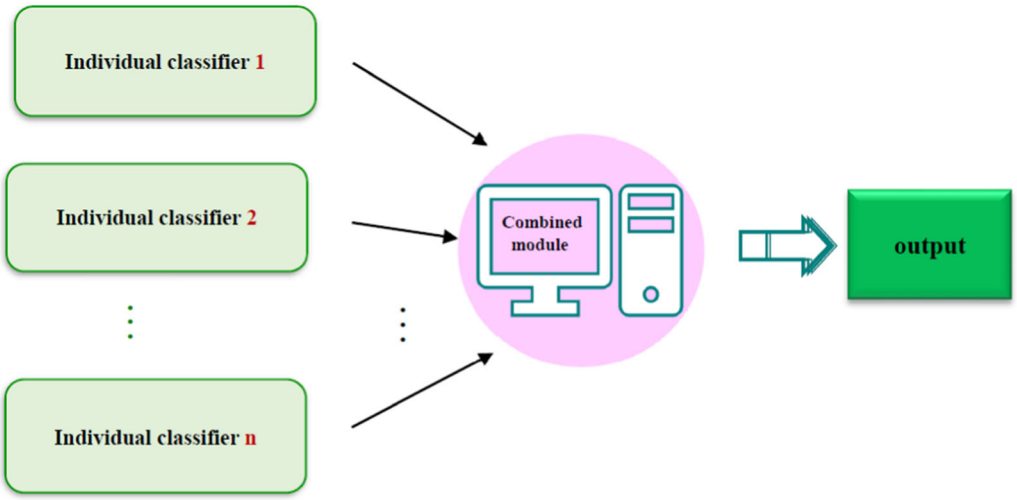

Fig. 1 Schematic diagram of ensemble learning

have been used in slope classification [58, 64] with good results; the resulting model allows rapid slope stability prediction. The following is only a brief introduction to each ensemble classification algorithm. For a more in-depth discussion, please refer to the relevant literature [23, 24].

2.1 Bagging

Bagging [4] is one of the simplest and most efficient ensemble learning algorithms. Figure 2 shows the structure diagram of bagging. First, m training samples are extracted from the original training samples. After the T-round extraction, T training sets can be obtained, and then the T training sets are used to train each 'weak learner'. Finally, each 'weak learner' result is combined according to the average or voting method. Each time the training set is extracted, all the features can be used for training, or some features can be randomly selected. There is no dependency among the 'weak learners', and they are all connected in parallel. Bagging can not only uniformly sample datasets but also realize parallel computing. For this reason, learners based on the bagging framework have better generalization ability and higher computing speed.

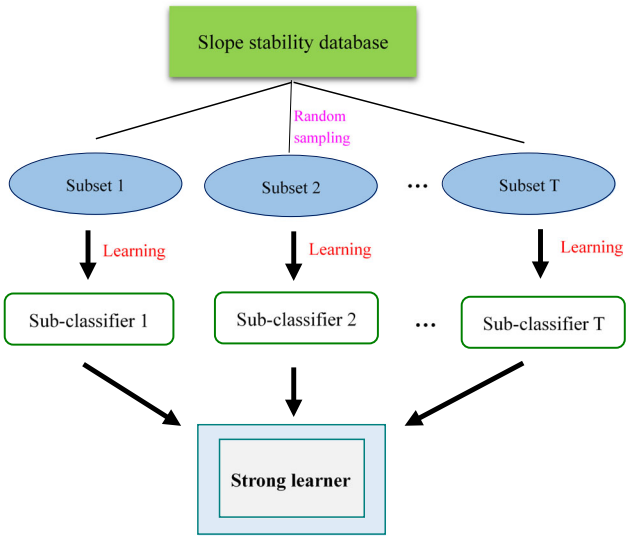

Fig. 2 Schematic diagram of bagging

2.2 Random forest

Random forest (RF) is a method based on bagging and decision trees (DTs) [19]. Unlike the traditional decision tree, RF randomly extracts n subsamples containing k attributes from the K attributes contained in N samples and then selects an optimal attribute from n subsamples for partitioning. RF combines the final prediction results based on the performance of multiple decision trees. RF can process high-dimensional data without feature selection and has strong adaptability to the dataset.

2.3 Boosting

Boosting [45] trains each 'weak learner' in an iterative manner. As shown in Fig. 3, 'weak learner 1' is trained on the original training set 1 and adjusts the training sample distribution according to its prediction results to obtain training set 2. Train on training set 2 to obtain 'weak learner 2'. The above process is repeated until the termination condition is satisfied, and the final prediction result is the weighted sum of the results of each base learner.

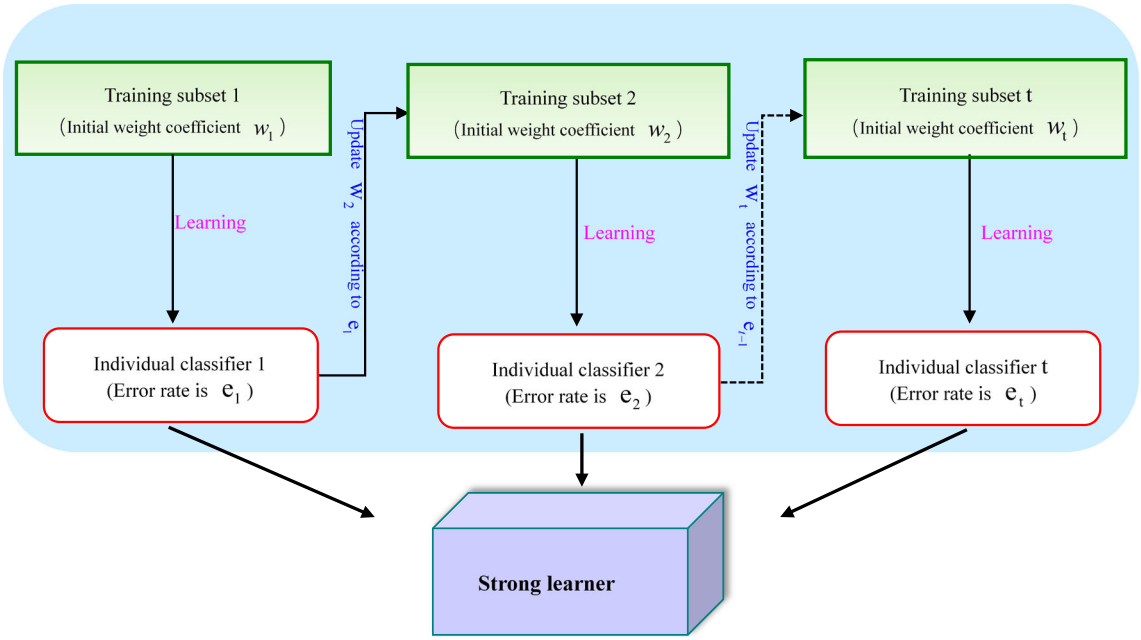

Fig. 3 Schematic diagram of boosting

Boosting is a forward distributed boosting algorithm. Each calculation step is affected by the previous step, and the weight of the miscalculated samples increases to improve the overall predictive ability of the algorithm model.

Adaptive boosting [17] (AdaBoost) is the most typical. AdaBoost can combine several low-precision classifiers and automatically adjust the sample weights according to the classification effect to synthesize a strong classifier with higher precision. AdaBoost is sensitive to outliers and noisy data.

2.4 Gradient boosting machine

The gradient boosting machine (GBM) [18] is a boosting algorithm. The GBM algorithm searches for weak classifiers along the gradient descent direction and trains an additive model to combine all weak classifiers. The loss function is used to express the fitting degree between the test set and training set. The lower the loss function is, the higher the prediction accuracy and the more reliable the result. GBM includes GBDT (gradient boosting decision tree), XGBoost (extreme gradient boosting), LightGBM (light gradient boosting machine) and CatBoost (categorical boosting).

Hist gradient boosting (HGB) [1], or histogram-based gradient boosting, is a boosting ensemble that uses feature histograms for fast and accurate selection of best splits. Light GBM inspires its implementation. HGB is more efficient than GBM in terms of memory consumption and processing speed.

2.5 Stacking

The stacking algorithm [53] has the advantages of simple structure, high performance and strong classification ability. The stacking structure diagram is shown in Fig. 4. The model of the first layer is called the base model, and the model of the second layer is called the meta-model. Using the predicted values of each model in the first layer as the input characteristics of the next layer, stacking has a stronger nonlinear expression ability than a single prediction model and can further reduce the generalization error. Based on the stacking algorithm, this paper uses GBM, RF, KNN, DT, SVC, LR, ET, bagging and Gaussian naive Bayes (GaussianNB) as the primary learners. LR is the secondary learner, and 10 times fivefold cross-training is used to avoid overfitting between the primary and second training models.

Stacking is a general method for achieving higher prediction accuracy by combining high-level models with low-level models. However, stacking generalization does not consider the data distribution and is suitable for standard datasets other than unbalanced data.

Bagging, boosting and stacking algorithms improve machine learning performance by merging multiple models. Bagging reduces model variance, boosting reduces

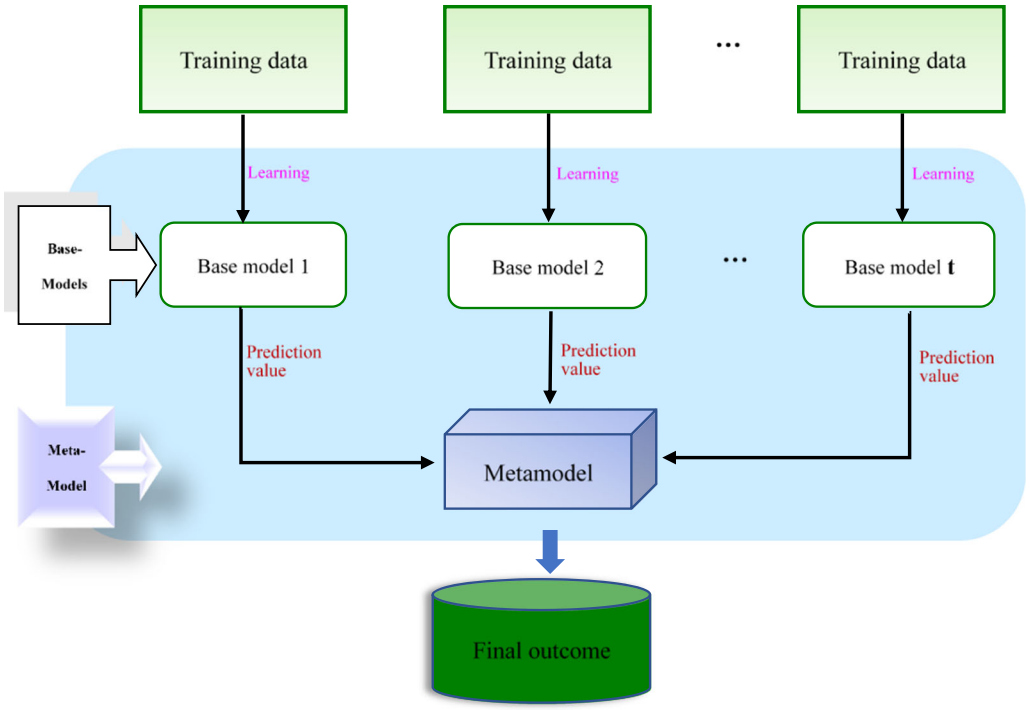

Fig. 4 Stacking schematic diagram

model deviation and stacking improves model prediction results.

2.6 Voting

The voting ensemble (majority vote set) is a machine learning model set that combines the predictions of several other models. Voting prediction classification methods include hard voting and soft voting. The hard vote set summarizes the votes from the clear class labels of other models and predicts the class with the most votes. A soft voting set includes the sum of predicted probabilities of the class labels and predicting the class label with a greater probability addition. Regardless of the machine learning model, the voting ensemble can be used and considered a meta-model. The voting method is fast and straightforward. It only requires the prediction results of the established model on the test dataset without retraining.

2.7 Extra trees

Extra trees (ET) [47] and RF have a similar structure. Unlike RF, ET uses the entire dataset to train each decision tree to utilize all samples fully. In addition, when ET trains T decision trees, N input features are randomly selected to form T subdatasets. In node partitioning, the subdataset is selected at random by the partition threshold of each characteristic, and the feature with the best partition effect is selected as the optimal partition attribute according to the specified threshold. According to the theory of 'error-ambiguity decomposition', the greater the difference between 'weak learners' and the higher the prediction accuracy of each 'weak learner', the better the integration effect. The size of the ET decision tree is generally larger than that of RF, but the variance in the model is minor.

3 Database and variables

3.1 Parameter analysis

When establishing the classification model, the factors affecting slope stability are selected first. The principles of feature selection are as follows: (a) the meaningful features are selected from the given feature set to train the model to reduce the dimension disaster problem; (b) the complexity of the learning process is simplified by removing some features that are not related to the subsequent learning process. At present, gravity γ, cohesion C, internal friction angle φ, slope angle β, slope height H and pore water ratio r_u have extensive use in slope stability prediction. According to the training, the results are good, and the data can easily be obtained [58]. It should be noted that according to engineering experience, the stability of the slope is also affected by other factors, such as the structure type of rock and soil, joints and the relationship between

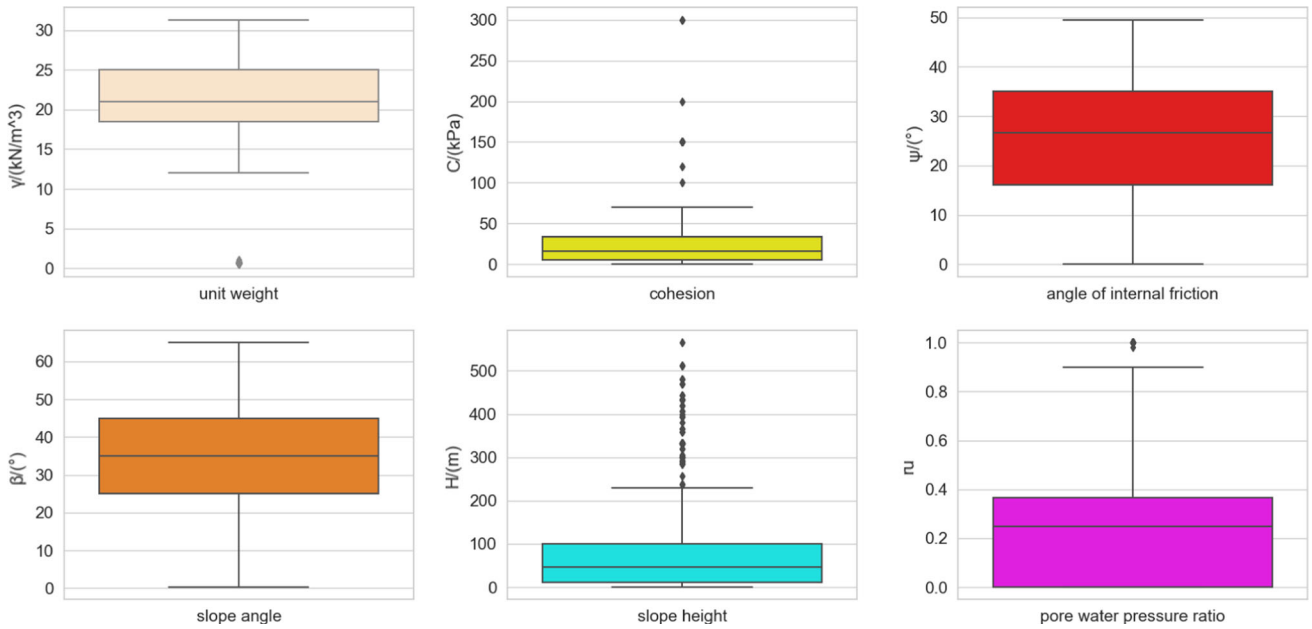

Fig. 5 Box plot of each variable for slope cases

the joint surface and slope angle. However, it is difficult to obtain the values of these indicators accurately. The results indicated that slope stability could be well predicted without considering these indices [64].

3.2 Case data and preliminary analysis

From a performance point of view, measurements and comparisons have been made for the ensemble learning algorithm, 444 engineering examples of slopes were collected directly from the literature [5–7, 14–16, 22, 26, 30, 31, 36, 37, 49, 51, 54–56, 68, 69], and all the data are from these studies without any processing. A detailed description of the data is provided in Appendix. As shown in Fig. 5, the box diagram describes all the input features used in the slope stability prediction model. From these figures, the range and average distribution of all input features can be found directly. Except for β, most variables have noncentre medians to the boxes. This indicates an asymmetric distribution of these variables. Additionally, except for φ and β, there are several outliers in all input features.

There are two types of slope stability in the dataset: stable (S, 224 cases) and unstable (F, 220 cases). The variable correlation matrix is shown in Fig. 6. There is a pairwise relationship between the correlation coefficients of the variables related to slope stability. The red lines outside the diagonal are regression lines, which reflect the degree of linear correlation between variables. The diagonal of the figure is the marginal frequency distribution of each parameter. The red lines on the diagonal represent the empirical probability density curves. The numbers in the upper panels indicate the correlation between the two variables. The red stars ('***', '**', '*;, '.', ' ') $< = > p$ values (0, 0.001, 0.01, 0.05, 0.1, 1). As shown in Fig. 6, the correlation is rather poor with most variables ($R < 0.5$). There is a significant correlation between γ and φ ($R = 0.73$), β ($R = 0.74$), a significant correlation between β and φ ($R = 0.70$), and a moderate correlation between γ and H ($R = 0.49$). r_u is negatively correlated with γ ($R = -0.20$) and φ ($R = -0.24$).

Furthermore, it is evident that the dataset is widely distributed and that the distribution of the variable is nonsymmetrical. Principal component analysis (PCA) summarizes and visualizes the collected slope data and explains its variance–covariance structure. As shown in Table 1, the contribution rate of PC1 is the highest, 52.26%, and the contribution rate of PC6 is the lowest, only 3.65%. PCA allows us to visualize the classification capabilities of the slope dataset on a two-dimensional plane. According to the PCA results (as shown in Fig. 7a), the components of the first and second dimensions were visualized (Fig. 7b). As shown in Fig. 7b, the data distribution regions of the two types of slope states on the first two components are relatively close, with overlapping areas. In addition, some indicators with significant skewness will affect the classification results of slope stability, as shown in Fig. 1. To avoid the interference of large

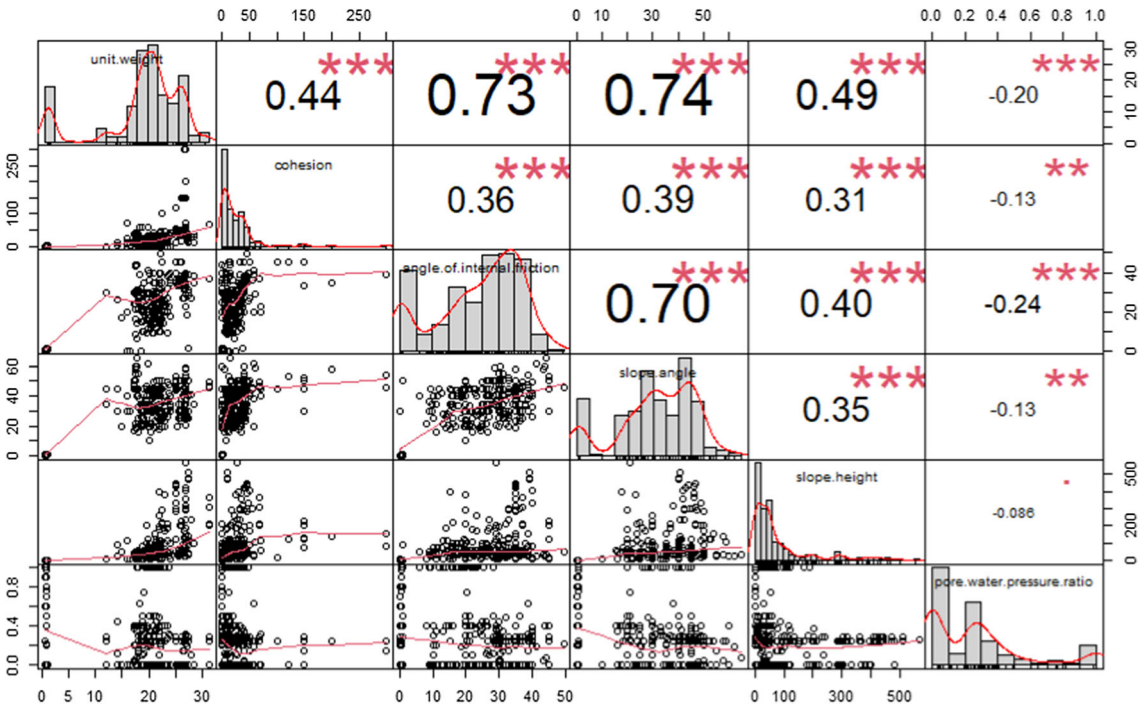

Fig. 6 Scatter matrix of the six variables of slope stability

Table 1 PCA model for illustration of the slope data: component matrix and scores

Principal component (PC)	Variable						Variance	Variance ratio (%)	Cumulative ratio (%)
	γ(kN/m^3)	C (kPa)	φ(°)	β(°)	H (m)	r_u			
PC1	0.5098	0.3462	0.4888	0.4787	0.3498	− 0.1723	3.1430	52.26	52.26
PC2	0.0609	0.0459	− 0.0232	0.1310	0.1968	0.9684	0.9517	15.82	68.08
PC3	− 0.1933	0.6583	− 0.3151	− 0.3700	0.5346	− 0.0852	0.7262	12.07	80.15
PC4	− 0.0440	0.6645	− 0.0079	0.1405	− 0.7258	0.0996	0.6976	11.60	91.75
PC5	0.1132	− 0.0507	− 0.7675	0.6150	0.0579	− 0.1181	0.2767	4.60	96.35
PC6	− 0.8272	0.0207	0.2685	0.4677	0.1518	− 0.0367	0.2193	3.65	100

fluctuation data on the model performance, when the difference in the order of magnitude of each control factor is too large or the same control factor is discrete, it is necessary to standardize the sample data. This article uses the Quantile Transformer function for data normalization.

Ideally, for the sake of precise classification, each value of all features can only have one class label (stable or failure) in the diagram. Slope stability is classified according to different indicators as shown in Fig. 8. It can be observed from this figure that, in some events, the same indicator's value corresponds to both types of slope states. The possible reason is that the data are not linearly separable and it is difficult to define boundaries of feature values.

4 Development of slope stability assessment model

4.1 Data pre-processing

To form and control the performance of the classifiers, as shown in Fig. 9, a stratified and random sampling method is used to split the dataset into training datasets (90%) and test datasets (10%). The tenfold cross-validation (CV) and grid search method are adopted to obtain optimal parameters of the ensemble learning models. In the process of tenfold CV, the training is divided into random tenfold training, nine of which are trained by the ensemble learning model, and the remaining training is used as the

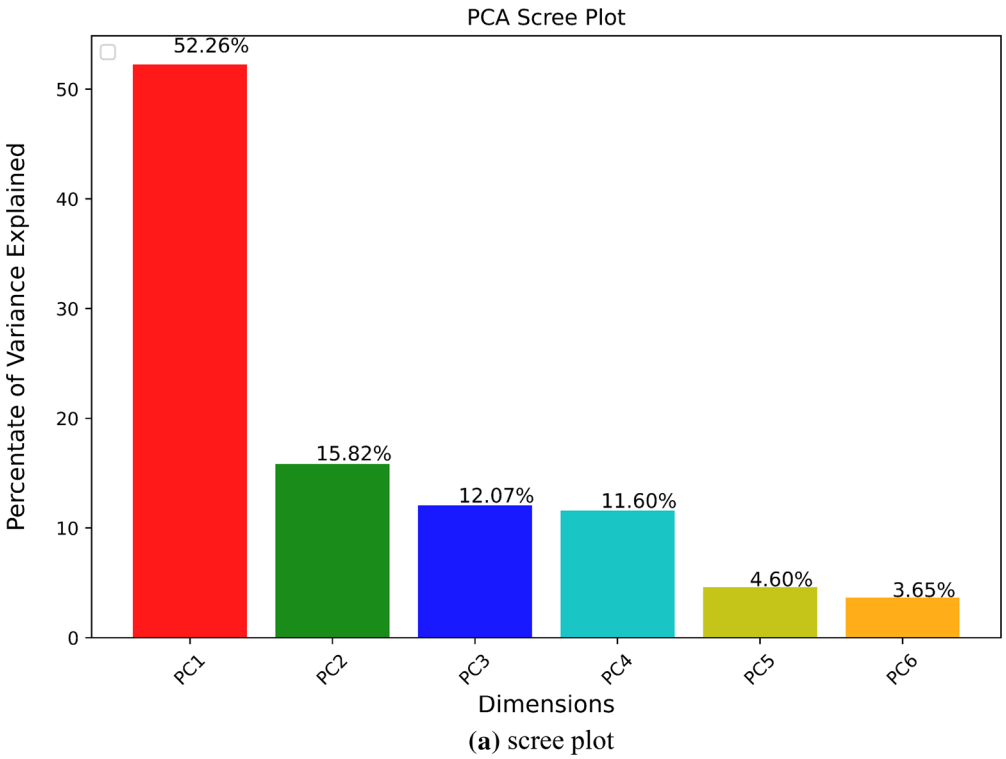

(a) scree plot

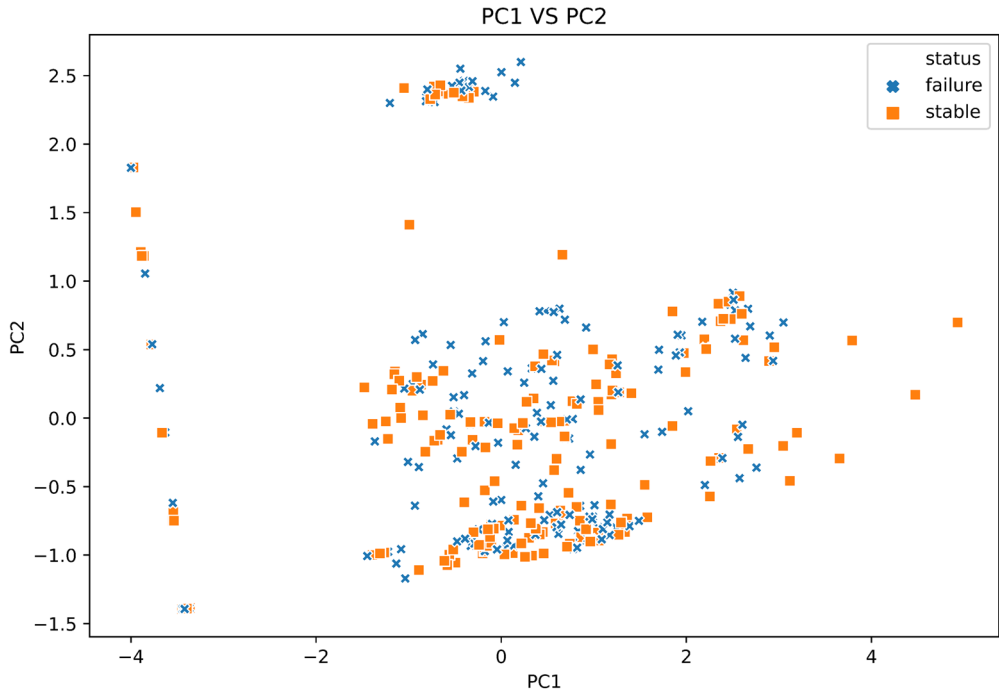

(b) a biplot of the first two components

Fig. 7 Visualization of PCA results

verification set to verify the model's performance. The training and testing process is repeated 10 times, and 10 different subsets are used as testing sets. Therefore, the overall performance of the ensemble learning algorithm on

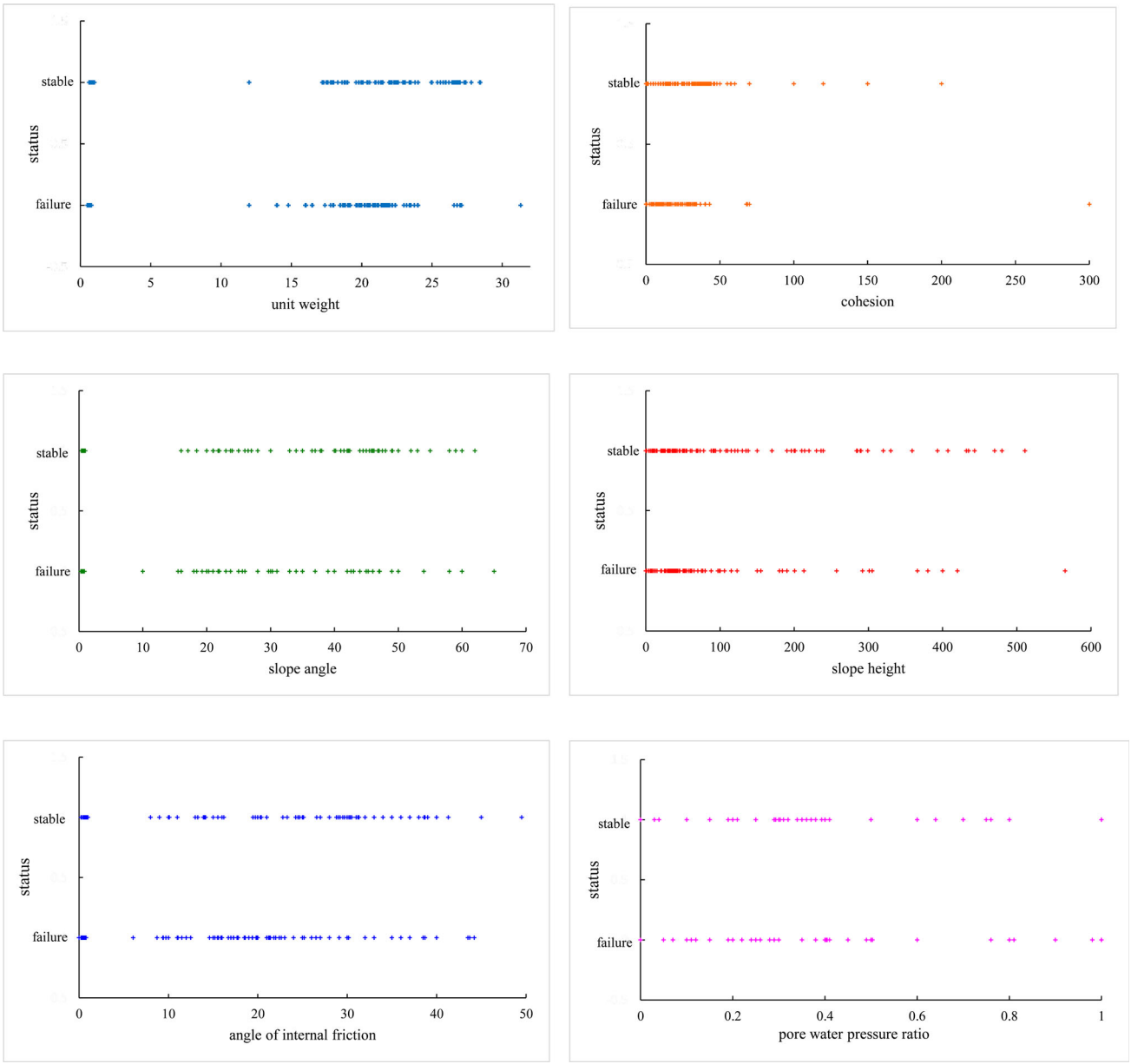

Fig. 8 Slope stability concerning each indicator

the training set is calculated by simply averaging the 10 training results.

4.2 Model performance evaluation

For slope stability classification problems, receiver operating characteristic (ROC) curves [3], log loss, accuracy and kappa coefficients [28] are the main indicators for evaluating the performance of classifiers. The ROC curve is a good comprehensive evaluation index without considering the sample distribution, making a credible performance evaluation of the algorithm results. The area under the curve (AUC) is enclosed by the ROC curve and the coordinate axis. AUC represents the probability that a positive sample is more likely to be predicted as a positive class than a negative sample to be a positive sample, which is often used to measure the classification performance of a classifier on unbalanced data. Different AUC values reflect different classification effects [3, 25]: 0.900–1.00 represents outstanding discrimination, 0.800–0.900 represents excellent discrimination, and 0.700–0.800 represents acceptable discrimination.

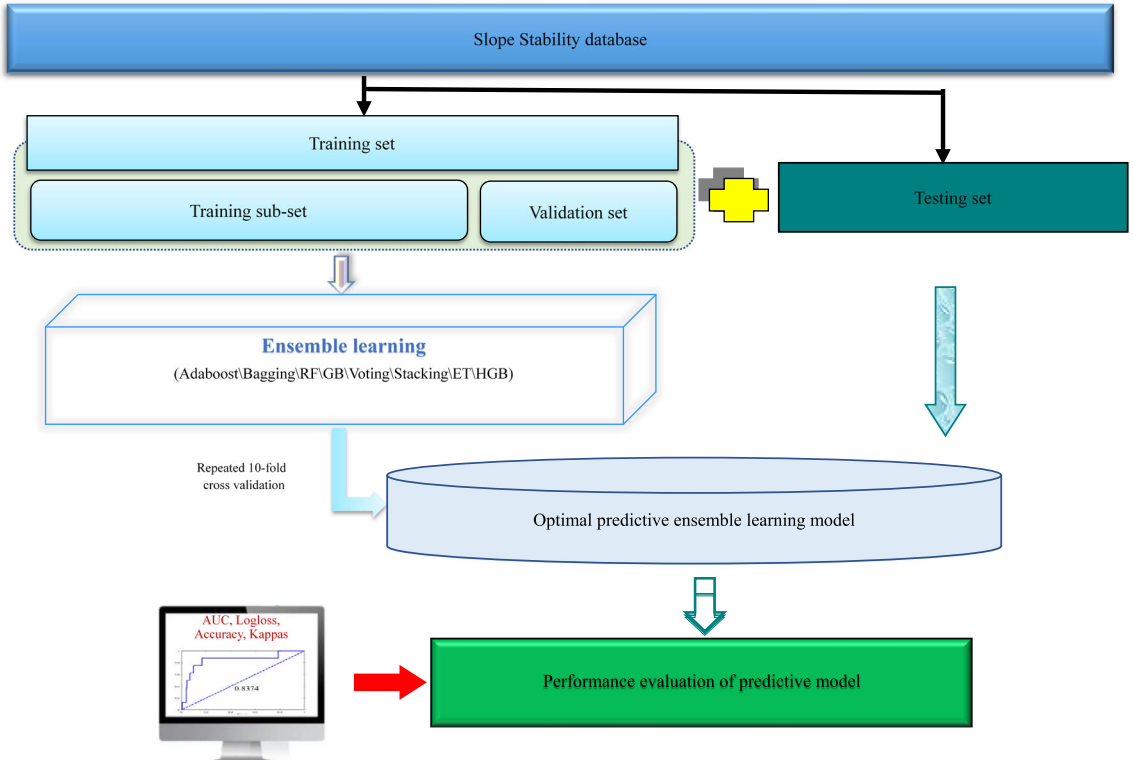

Fig. 9 Ensemble learning model for predicting slope stability

Log loss is a performance metric used to evaluate the probability of members of a given class. The log loss can be given using Eq. 1.

$$\log\text{loss} = -\frac{1}{n}\sum_{i=1}^{n}\sum_{j=1}^{m} y_{ij}\log(p_{ij}) \tag{1}$$

where n represents the total number of samples and m is the number of types of slope stability. When sample i belongs to class j, y_{ij} is 1; otherwise, y_{ij} is 0. Furthermore, p_{ij} represents the probability of sample i belonging to class j. For a binary classification problem, the log loss function is as follows:

$$-\log\text{loss} = -\sum_{i=1}^{n}\left(y_i\log(p_i) + (1-y_i)\log(1-p_i)\right) \tag{2}$$

Accuracy is defined as the percentage of the number of samples correctly classified relative to the total number of samples selected for validation, and Eq. 3 calculates the precision. The accuracy can reflect the overall classification accuracy to a certain extent but cannot directly reflect the different classes' prediction results. The kappa coefficient is a comprehensive classifier evaluation index [63] mainly used to reflect the proportion of error reduction compared with random classification. Equation 4 is the expression of kappa.

$$\text{Accuracy} = \left(\frac{1}{n}\sum_{i=1}^{r} z_{ii}\right) \times 100\% \tag{3}$$

$$\text{Kappa} = \left[n\sum_{i}^{r} z_{ii} - \sum\left(z_{i+}z_{+i}\right)\right] \Big/ n^2 - \sum\left(z_{i+}z_{+i}\right) \tag{4}$$

where r represents the number of categories to be classified by the confusion matrix. z_{ii} is the value of row i and column i of the confusion matrix, the number of samples correctly classified; z_{i+} and z_{+i} represent the sums of row i and column i, respectively, of the confusion matrix.

The distribution range of the kappa coefficient is [− 1,1], where − 1 represents the worst classification effect, 0 represents the classification performance of the classifier equal to the random classifier and 1 represents the best classification performance. Different kappa coefficients reflect different classification effects: 0.810–1.000 (perfect), 0.610–0.800 (substantial), 0.410–0.600 (moderate), 0.210–0.400 (poor), 0.000–0.200 (slight) and − 1.000–0.000 (total disagreement). Generally, 0.4 is taken as the threshold of the kappa coefficient [63].

Table 2 Tuning parameters of each model for an optimal classification

Method	Turning parameters	Optimal value	AUC	Sensitivity	Specificity
GBM	n_estimators = [10, 50, 100, 500]	100	0.9199	0.8421	0.9130
	learning_rate = [0.0001, 0.001, 0.01, 0.1, 1.0]	0.1			
	subsample = [0.5, 0.7, 1.0]	1.0			
	max_depth = [20, 33, 65]	7			
Bagging	n_trees = [10, 50, 100, 500, 1000, 5000]	100	0.9291	0.7895	0.8696
	max_samples = [0.1, 0.3, 0.5, 0.7, 0.9,1]	1			
	max_features = 2,3,4,5	3			
AdaBoost	n_estimators = [10, 50, 100, 500]	500	0.9199	0.8421	0.8261
	learning_rate = [0.0001, 0.001, 0.01, 0.1, 1.0]	1.0			
ET	min_samples_split = [13, 35, 38, 48, 59, 60, 67, 70]	6	0.9519	0.8947	0.9565
	max_features = [13, 20, 60, 61]	3			
	n_trees = [10, 50, 100, 500, 1000, 5000]	100			
RFC	max_samples = [0.2, 0.4, 0.6, 0.8, 1]	1	0.9268	0.7894	0.8696
	max_features = [13, 20, 60, 61]	3			
	n_trees = [10, 50, 100, 500, 1000]	100			
HGB	None	None	0.8970	0.7368	0.9130
Voting	None	None	0.9588	0.8421	0.9565
Stacking	None	None	0.9382	0.8421	0.9565

4.3 Model development and parameter optimization

This paper studies the applicability of eight common ensemble learning algorithms (GBM, AdaBoost, bagging, ET, RF, HGB, voting and stacking) in slope stability classification. Most classifiers (GBM, AdaBoost, bagging, ET and RF) contain parameters that need to be adjusted. The 'gridsearchcv' function in sklearn performs a tuning parameter grid for many classification problems, which allows a single consistent environment to train each ensemble learning method and tune their related parameters. After evaluating the optimal parameters, the final slope stability prediction models are established using the entire training dataset. To optimize the critical parameters of each integrated training model and obtain the best discrimination performance, a tenfold reputation of CV is used to select the 'optimal' value of the adjustment parameter. As a binary classification problem, slope stability is a trade-off between sensitivity and specificity. AUC represents the model's ability to distinguish between positive (stable) and negative (failure) categories. Therefore, the AUC is used to evaluate the performance of the parameters in the repeated tenfold CV process. Table 2 shows the hyperparameter settings and prediction results of the ensemble learning algorithms in the current research.

5 Results and discussion

5.1 Discriminant results and performance analysis

To compare the performance of different classification algorithms, the KNN, LR, GaussianNB, MLPClassifier (MLPC) and SVM methods are also used for slope stability classification. The prediction results of the model are shown in Fig. 10. The AUC of SVM is 0.898, LR is 0.752, KNN is 0.934, GaussianNB is 0.695, MLPC is 0.839, RF is 0.967, GBM is 0.961, ET is 0.966, AdaBoost is 0.961, bagging is 0.965 and HGBC is 0.959. It is worth noting that the AUC determines the classifier's performance greatly, and 1.0 represents the ideal performance. The ROC curves of ensemble learning (RF, GBM, ET, AdaBoost, bagging and HGB) are slightly more approximated to the left and upper axes than the other models. Their AUC values were above 0.90, slightly higher than those of KNN, and significantly higher than those of SVM, LR and MLPC. It also shows that ensemble learning is more suitable for slope stability prediction, and GaussianNB has the lowest prediction performance. The AUC value of the ensemble learning model constructed by the average predicted value of SVM, LR, KNN, GaussianNB, MLPC, RF, GBM, ET, AdaBoost, bagging and HGB is 0.961. These facts convincingly demonstrate that ensemble learning has a good ability to predict slope stability.

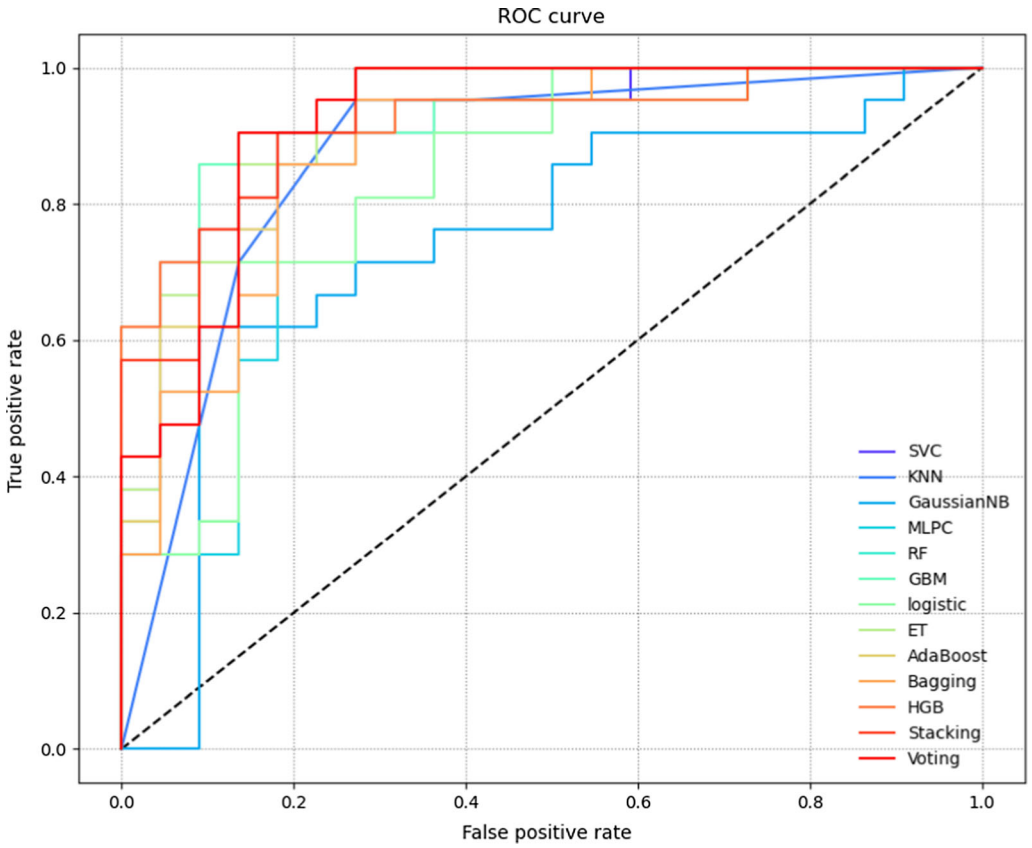

Fig. 10 ROC curves of the thirteen classifiers on the testing set

According to the visual comparison, one can easily observe the performance of all the ensemble learning classification methods, as shown in Figs. 11 and 12. The boxplots in Fig. 11 report the performance of eight classifiers on a repeated tenfold CV procedure with average AUC, accuracy, log loss and kappa. Since these models use the same dataset, it is meaningful to analyse the differences between the calculated results. The distinction of the upper and lower quartiles in the stacking classifier is smaller than that of the other methods, indicating that the accuracy variance is relatively low in different iterations (see Fig. 11). Figure 12 shows that the average AUC of each ensemble classifier in slope stability prediction is between [0.8992–0.9452]. The stacking model has the highest AUC, with an AUC of 0.9452, followed by the GBM method (AUC = 0.9293), RF method (AUC = 0.9210) and ET method (AUC = 0.9180). According to the consistency scale, the AUCs of all modelling techniques used in the model evaluation test set are excellent. As shown in Fig. 11, the accuracy and kappa value of stacking have the closest quartile range. The quartile range of the ROC value of GBM is the closest, but there are some outliers. The average value of log loss of each ensemble classifier in slope stability prediction falls into [0.3282–0.6860]. The lowest log loss is the stacking model, and the log loss is 0.3282, followed by the RF method (log loss = 0.3776) and ET method (log loss = 0.3894). Smaller log loss is better, with 0 representing a perfect log loss. AdaBoost performed relatively worse, with a log loss of 0.6860.

The average accuracy of the ensemble classifiers in slope stability prediction falls into the range of [82.07–84.74%]. Obviously, the accuracy of the stacking model is the highest (accuracy = 84.74%), and then the ET (accuracy = 83.53%), bagging (accuracy = 83.07%) and GBM (accuracy = 82.81%) models rank successively. Voting achieves the lowest average accuracy (82.07%). For the eight ensemble learning techniques, the performance (in terms of average kappa) falls into the range of (0.6377–0.8474). The kappa values of all ensemble learning models are above 0.4. The stacking predictor achieves the highest kappa (0.6910), followed by ET, bagging and

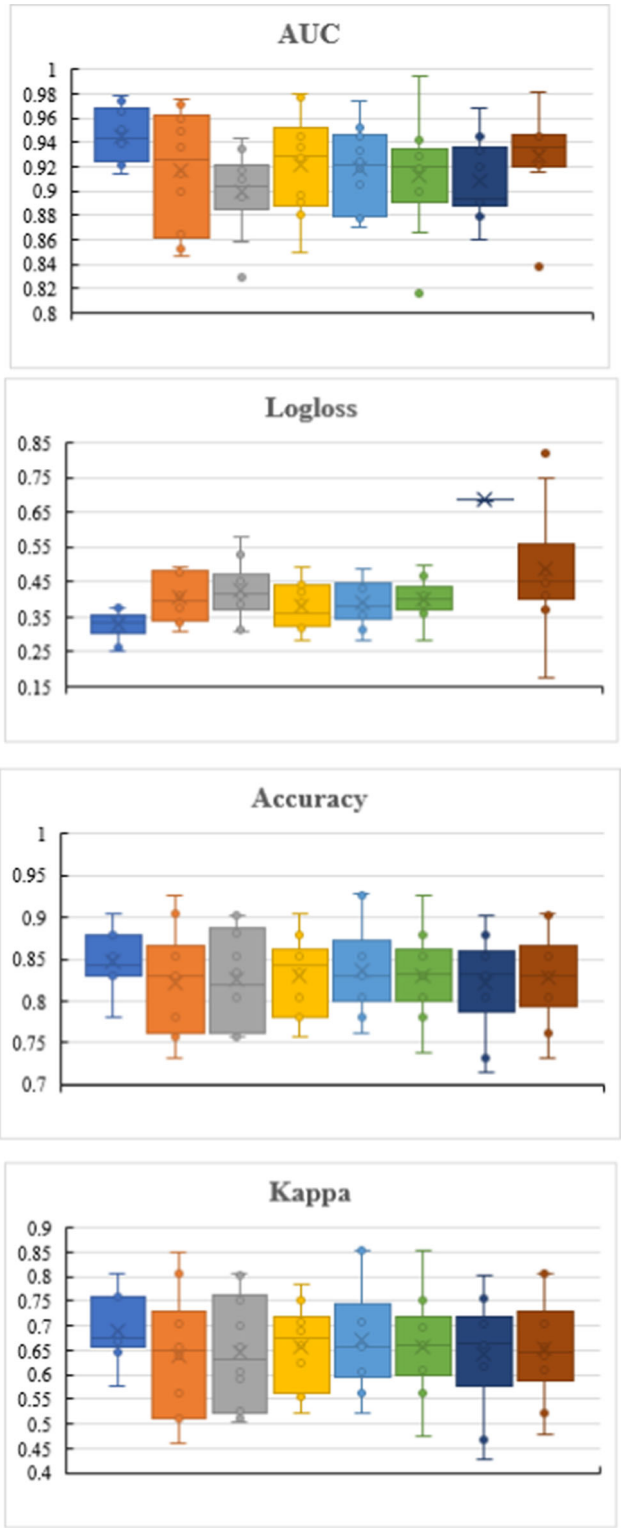

Fig. 11 Boxplot distributions of the training set in terms of 'AUC', 'log loss', 'accuracy' and 'kappa' for eight ensemble methods resulting from repeated tenfold CV procedure

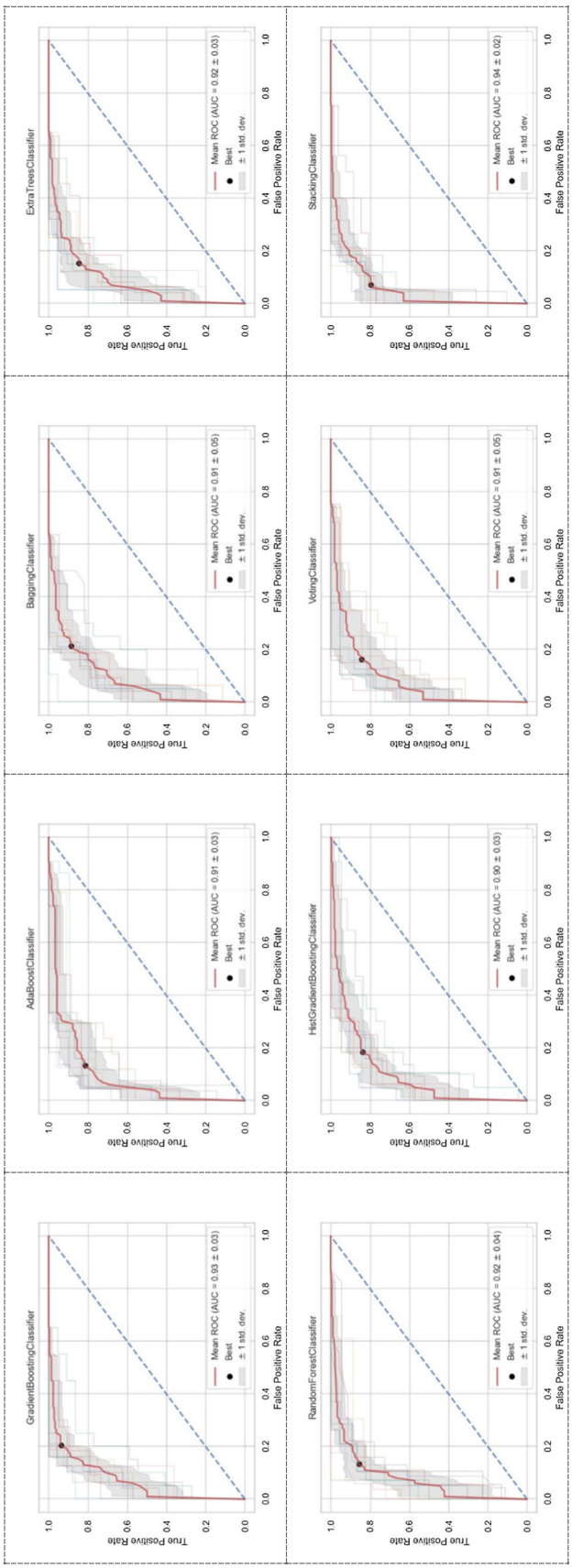

Fig. 12 ROC curves for the ensemble models

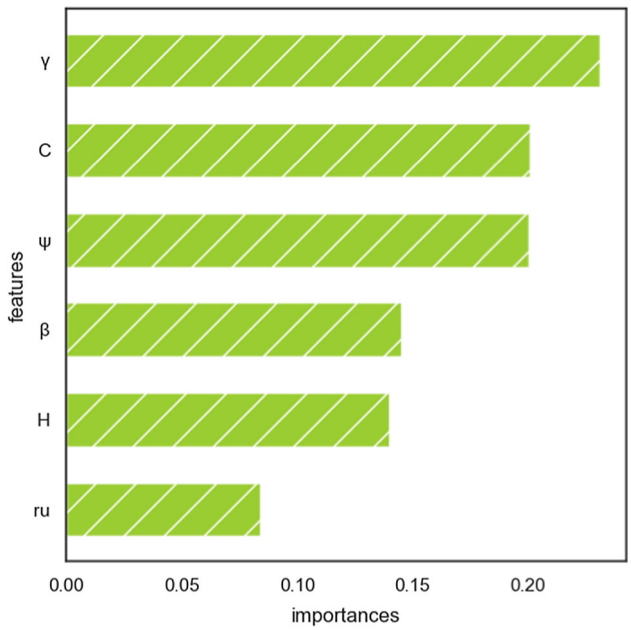

Fig. 13 Variable importance plot generated by the GBM, ET and RF classifiers

GBM, with average kappa rates of 0.6703, 0.6590 and 0.6545, respectively.

According to the concordance scale, the kappa of the training set and test set of eight ensemble learning classification techniques in model calibration data is medium to substantial. It is clear that the kappa and accuracy of each ensemble learning classification algorithm are basically the same, but kappa is usually smaller than accuracy. The reason is that kappa can more comprehensively reflect the error information of the model, while accuracy only considers the diagonal element error in the confusion matrix and ignores the element error on the nondiagonal line.

The results show that ensemble learning models have good performance in predicting slope stability, which is feasible and reliable. We can observe the following facts. Compared with a single classifier, the stacking ensemble classifier has a relatively higher average AUC (0.9452), average accuracy (84.74%) and kappa average (0.6910) and a relatively lower average log loss (0.3282) on the testing set, indicating that its prediction performance is relatively higher, but the calculation intensity is high, and it takes the longest time to train; stacking has better generalization performance than voting. This research indicates that using a classifier ensemble, rather than searching for the ideal single classifier, may be more helpful for slope stability prediction.

5.2 Relative variable impact

Determining the sensitivity of the factors affecting slope stability is very important for evaluating slope stability and the design of support structures. A relative importance score is used in this study, and this is based on optimal ensemble learning (GBM, ET and RF) to study the sensitivity. The methods are selected according to their excellent performance on the test set. The variable importance ranking is obtained by averaging the tenfold CV feature selection results of RF, ET and GBM. Figure 13 shows the normalized score of variable importance. γ (score = 0.2309), C (score = 0.2007) and φ (score = 0.2003) are the most sensitive factors to slope stability, which indicates the importance of slope material variables. The correlation matrix of the variables is consistent with these results (Fig. 6), the component matrix and scores, and the literature results [52]. Therefore, the values of the material γ, C and φ in artificial slopes must be reasonably and accurately selected based on specific indoor and field tests. In treating landslides, geomaterials' cohesive force and internal friction angle should be improved [39]. The importance scores of β and H are 0.1449 and 0.1395, respectively, indicating that geometric variables also affect slope stability. Optimizing these two variables in practical design is a feasible method for ensuring slope stability. It can also be found that the sensitivity of r_u (0.0837) is not as good as that of the first five features.

6 Conclusions

Ensemble learning algorithms (GBM, AdaBoost, bagging, ET, RF, HGB, voting and stacking) are introduced in this study to study the stability of 444 slope cases. Six potential relevant indicators, γ, C, φ, β, H and r_u, serve as indicators for prediction, and the generalization ability of the classification models is improved using the tenfold CV method. According to the analyses, the following conclusions are presented:

1. The ROC curves of ensemble learning algorithms are closer to the left and top axes than other algorithms. The AUC of ensemble learning models is more than 0.900, slightly higher than KNN, SVM, LR and MLPC. The AUC value of the ensemble learning model constructed by the average predicted value of SVM, LR, KNN, GaussianNB, MLPC, RF, GBM, ET, AdaBoost, bagging and HGBC is 0.961. Ensemble learning algorithms have an excellent ability to predict slope stability.
2. The stacking model has a higher AUC, higher accuracy and kappa value, and lower log loss. It can be used as a

Table 3 Slope stability prediction database

NO	r (kN/m^3)	C (kPa)	φ (°)	β (°)	H (m)	r_u	Status	Location
1	18.68	26.34	15	35	8.23	0	Failure	Congress street, open cut slope, Chicago, USA
2	16.5	11.49	0	30	3.66	0	Failure	Brightlingsea slide, UK
3	18.84	14.36	25	20	30.5	0	Stable	Unknown
4	18.84	57.46	20	20	30.5	0	Stable	Unknown
5	28.44	29.42	35	35	100	0	Stable	Case 1: open-pit iron ore mine, India
6	28.44	39.23	38	35	100	0	Stable	Case 2: open-pit iron ore mine, India
7	20.6	16.28	26.5	30	40	0	Failure	open-pit chromite mine, Orissa, India
8	14.8	0	17	20	50	0	Failure	Sarukuygi landslide, Japan
9	14	11.97	26	30	88	0	Failure	Case 1: open-pit iron ore mine, Goa, India
10	25	120	45	53	120	0	Stable	Mercoirol open-pit coal mine, France
11	26	150.05	45	50	200	0	Stable	Marquesade open-pit iron ore mine, Spain
12	18.5	25	0	30	6	0	Failure	Unknown
13	18.5	12	0	30	6	0	Failure	Unknown
14	22.4	10	35	30	10	0	Stable	Case 1: Highvale coal mine, Alberta, Canada
15	21.4	10	30.34	30	20	0	Stable	Case 2: Highvale coal mine, Alberta, Canada
16	22	20	36	45	50	0	Failure	Case 1: open-pit coal mine, Newcastle coalfield, Australia
17	22	0	36	45	50	0	Failure	Case 2: open-pit coal mine, Newcastle coalfield, Australia
18	12	0	30	35	4	0	Stable	Unknown
19	12	0	30	45	8	0	Failure	Unknown
20	12	0	30	45	4	0	Stable	Unknown
21	12	0	30	45	8	0	failure	Unknown
22	23.47	0	32	37	214	0	Stable	Pima open-pit mine, Arizona, USA
23	16	70	20	40	115	0	Failure	Case 1: Wyoming, USA
24	20.41	33.52	11	16	10.67	0.35	Stable	Seven Sisters Landslide, UK
25	19.63	11.97	20	22	12.19	0.405	Failure	Case 1: The Northolt slide, UK
26	21.82	8.62	32	28	12.8	0.49	Failure	Selset Landslide, Yorkshire, UK
27	20.41	33.52	11	16	45.72	0.2	Failure	Saskatchewan dam, Canada
28	18.84	15.32	30	25	10.67	0.38	Stable	Case 2: The Northolt slide, UK
29	18.84	0	20	20	7.62	0.45	Failure	Sudbury slide, UK
30	21.43	0	20	20	61	0.5	Failure	Folkestone Warren slide, Kent, UK
31	19.06	11.71	28	35	21	0.11	Failure	River bank side, Alberta, Canada
32	18.84	14.36	25	20	30.5	0.45	Failure	Unknown
33	21.51	6.94	30	31	76.81	0.38	Failure	Unknown
34	14	11.97	26	30	88	0.45	Failure	Case 2: open-pit iron ore mine, Goa, India
35	18	24	30.15	45	20	0.12	Failure	Athens slope, Greece
36	23	0	20	20	100	0.3	Failure	Open-pit coal mine Allori coalfield, Italy
37	22.4	100	45	45	15	0.25	Stable	Case 1: open-pit coal mine, Alberta, Canada
38	22.4	10	35	45	10	0.4	Failure	Case 2: open-pit coal mine, Alberta, Canada
39	20	20	36	45	50	0.25	Failure	Case 3: open-pit coal mine, Newcastle coalfield, Australia
40	20	20	36	45	50	0.5	Failure	Case 4: open-pit coal mine, Newcastle coalfield, Australia
41	20	0	36	45	50	0.25	Failure	Case 5: open-pit coal mine, Newcastle coalfield, Australia
42	20	0	36	45	50	0.5	Failure	Case 6: open-pit coal mine, Newcastle coalfield, Australia
43	22	0	40	33	8	0.35	Stable	Case 1: Harbour slope, Newcastle, Australia
44	24	0	40	33	8	0.3	Stable	Case 2: Harbour slope, Newcastle, Australia
45	20	0	24.5	20	8	0.35	Stable	Case 3: Harbour slope, Newcastle, Australia
46	18	5	30	20	8	0.3	Stable	Case 4: Harbour slope, Newcastle, Australia
47	22	29	15	18	400	0	Failure	Qing River area landslide, China
48	23	24	19.8	23	380	0	Failure	Qing River area landslide, China
49	22	40	30	30	196	0	Stable	Qing River area landslide, China
50	22.54	29.4	20	24	210	0	Stable	Qing River area landslide, China
51	22	21	23	30	257	0	Failure	Qing River area landslide, China
52	23.5	10	27	26	190	0	Failure	Qing River area landslide, China
53	22.5	18	20	20	290	0	Stable	Qing River area landslide, China

Table 3 (continued)

NO	r (kN/m^3)	C (kPa)	φ (°)	β (°)	H (m)	r_u	Status	Location
54	22.5	20	16	25	220	0	Stable	Qing River area landslide, China
55	18.68	26.34	15	35	8.23	0	Failure	Qing River area landslide, China
56	16.05	11.49	0	30	3.66	0	Failure	Qing River area landslide, China
57	18.84	14.36	25	20	30.5	0	Stable	Qing River area landslide, China
58	28.44	29.42	35	35	100	0	Stable	Qing River area landslide, China
59	28.44	39.23	38	35	100	0	Stable	Qing River area landslide, China
60	20.6	16.28	26.5	30	40	0	Failure	Qing River area landslide, China
61	14.8	0	17	20	50	0	Failure	Qing River area landslide, China
62	14	11.97	26	30	88	0	Failure	Qing River area landslide, China
63	25	12	45	53	120	0	Stable	Qing River area landslide, China
64	26	15	45	50	200	0	Stable	Qing River area landslide, China
65	16	7	20	40	115	0	Failure	Qing River area landslide, China
66	20.41	24.9	13	22	10.67	0	Stable	Qing River area landslide, China
67	19.63	11.98	20	22	12.19	0	Failure	Qing River area landslide, China
68	21.83	8.62	32	28	12.8	0	Failure	Qing River area landslide, China
69	20.41	33.52	11	16	45.72	0	Failure	Qing River area landslide, China
70	18.84	15.32	30	25	10.67	0	Stable	Qing River area landslide, China
71	18.84	0	20	20	7.62	0	Failure	Qing River area landslide, China
72	21.43	0	20	20	61	0	Failure	Qing River area landslide, China
73	20	8	20	10	10	0	Failure	Slope in Tailie elementary school
74	27.3	37.3	31	30	30	0	Stable	Slope on the right of Circle E of Tailie Overpass
75	20.6	26.31	22	25	35	0	Failure	Landslide on the left of K71 + 625 ~ K71 + 700
76	21.6	6.5	19	40	50	0	Failure	Slope of Pingxite Bridge
77	22.4	28.9	24	28	35	0	Failure	Slope on the right of K76 + 085 ~ K76 + 200
78	23.2	31.2	23	30	33	0	Failure	Slope on the left of K77 + 920 ~ K78 + 100
79	26.8	37.5	32	30	26	0	Stable	Slope on the left of K79 + 165 ~ K79 + 300
80	27.4	38.1	31	25	42	0	Stable	Slope on the right of K79 + 920 ~ K80 + 035
81	21.8	32.7	27	50	50	0	Failure	Landslide on the right of ZAK0 + 315 ~ ZAK0 + 407
82	21.8	27.6	25	35	60	0	Failure	Slope on the left of K83 + 260 ~ K83 + 360
83	26.5	35.4	32	30	21	0	Stable	Slope on the right of K88 + 300 ~ K88 + 420
84	26.5	36.1	31	35	39	0	Stable	Slope on the right of K88 + 700 ~ K88 + 876
85	27	35.8	32	30	69	0	Stable	Slope on the right of K89 + 730 ~ K89 + 841
86	27	38.4	33	25	22	0	Stable	Slope on the right of K90 + 225 ~ K90 + 345
87	21.4	28.8	20	50	52	0	Failure	Slope on the left of K98 + 520 ~ K98 + 710
88	26	42.4	37	38	55	0	Stable	Slope on the left of K99 + 120 ~ K99 + 260
89	26	39.4	36	25	30	0	Stable	Slope on the left of K100 + 280 ~ K100 + 410
90	25.6	38.8	36	25	26	0	Stable	Slope on the left of K100 + 615 ~ K100 + 915
91	20	30.3	25	45	53	0	Failure	Landslide on the left of K103 + 330 ~ K103 + 450
92	25.8	34.7	33	30	50	0	Stable	Slope on the left of K104 + 610 ~ K104 + 805
93	21.8	28.8	26	35	99	0	Failure	Landslide on the left of K104 + 892 ~ K105 + 052
94	21.8	31.2	25	30	60	0	Failure	Landslide on the left of K105 + 260 ~ K105 + 330
95	24	41.5	36	30	51	0	Stable	Slope on the left of K106 + 268 ~ K106 + 577
96	24	40.8	35	35	50	0	Stable	Slope on the left of K106 + 992 ~ K107 + 085
97	20.6	27.8	27	35	70	0	Failure	Landslide on the left of K107 + 856 ~ K107 + 968
98	20.6	32.4	26	35	55	0	Failure	Landslide on the left of K108 + 960 ~ K109 + 010
99	25.8	38.2	33	27	40	0	Stable	Slope on the left of K109 + 841 ~ K109 + 900
100	25.8	39.4	33	25	45	0	Stable	Slope on the left of K110 + 200 ~ K110 + 274
101	21.1	33.5	28	40	31	0	Failure	Landslide on the left of K110 + 421 ~ K110 + 500
102	21.1	34.2	26	30	75	0	Failure	Landslide on the left of K110 + 980 ~ K110 + 240
103	26.6	42.4	37	25	52	0	Stable	Slope on the right of K112 + 720 ~ K112 + 815
104	26.6	44.1	38	35	42	0	Stable	Slope on the left of K113 + 500 ~ K113 + 580
105	26.6	40.7	35	35	60	0	Stable	Slope on the left of K114 + 060 ~ K114 + 167
106	25.8	41.2	35	30	40	0	Stable	Slope on the left of K114 + 224 ~ K114 + 258

Table 3 (continued)

NO	r (kN/m^3)	C (kPa)	φ (°)	β (°)	H (m)	r_u	Status	Location
107	25.8	43.3	37	30	33	0	Stable	Slope on the left of K117 + 200 ~ K117 + 412
108	21.7	32	27	45	60	0	Failure	Front slope of tunnel in SongjieyaK122 + 310
109	20.6	28.5	27	40	65	0	Failure	Landslide on the right of K122 + 350 ~ K122 + 455
110	21.5	29.8	26	40	70	0	Failure	Landslide on the left of K127 + 440 ~ K127 + 590
111	26.5	42.9	38	34	36	0	Stable	Slope on the left of K127 + 761 ~ K127 + 882
112	20.8	15.6	20	30	45	0	Failure	Landslide on the left of K137 + 650 ~ K137 + 730
113	20.8	14.8	21	30	40	0	Failure	Landslide on the left of K138 + 624 ~ K138 + 797
114	19.6	29.6	23	40	58	0	Failure	Landslide on the right of K75 + 760 ~ K76 + 000
115	25.4	33	33	20	35	0	Stable	Slope on the right of ZBK0 + 000 ~ ZBK0 + 185
116	22.4	29.3	26	50	50	0	Failure	Landslide on the left of K84 + 602 ~ K85 + 185
117	26.2	41.5	36	35	30	0	Stable	Slope on the right of K91 + 614 ~ K91 + 660
118	26.2	42.3	36	23	36	0	Stable	Slope on the right of K91 + 720 ~ K91 + 771
119	25.6	39.8	36	30	32	0	Stable	Slope on the left of K100 + 950 ~ K101 + 300
120	25.6	36.8	34	35	60	0	Stable	Slope on the left of K102 + 691 ~ K102 + 880
121	26.2	42.8	37	30	37	0	Stable	Slope on the right of K118 + 360 ~ K118 + 549
122	26.2	43.8	38	35	68	0	Stable	Slope on the right of K119 + 823 ~ K119 + 951
123	20.6	32.4	26	30	42	0	Failure	Landslide on the right of K124 + 340 ~ K124 + 562
124	26.5	41.8	36	42	54	0	Stable	Slope on the right of K131 + 280 ~ K131 + 380
125	20.8	15.4	21	30	53	0	Failure	Landslide on the left of K138 + 840 ~ K138 + 930
126	27.3	14	31	41	110	0.25	Stable	Circular critical failure mechanism
127	27.3	31.5	30	41	135	0.25	Stable	Circular critical failure mechanism
128	27.3	16.8	28	50	90.5	0.25	Stable	Circular critical failure mechanism
129	27.3	26	31	50	92	0.25	Stable	Circular critical failure mechanism
130	18.5	25	0	30	6	0.25	Failure	Circular critical failure mechanism
131	18.5	12	0	30	6	0.25	Failure	Circular critical failure mechanism
132	22.4	10	35	30	10	0.25	Stable	Circular critical failure mechanism
133	21.4	10	30	30	20	0.25	Stable	Circular critical failure mechanism
134	22	0	36	45	50	0.25	Stable	Circular critical failure mechanism
135	12	0	30	45	4	0.25	Stable	Circular critical failure mechanism
136	12	0	30	45	8	0.25	Failure	Circular critical failure mechanism
137	12	0	30	45	4	0.25	Stable	Circular critical failure mechanism
138	18.66	8.8	15	35	8.2	0	Failure	Circular critical failure mechanism
139	28.4	9.8	35	35	100	0	Stable	Circular critical failure mechanism
140	25.96	50	45	50	200	0	Stable	Circular critical failure mechanism
141	18.46	8.35	0	30	6	0	Failure	Circular critical failure mechanism
142	21.36	3.35	30	30	20	0	Stable	Circular critical failure mechanism
143	15.99	23.35	20	40	115	0	Failure	Circular critical failure mechanism
144	20.39	8.3	13	22	10.6	0.35	Stable	Circular critical failure mechanism
145	19.6	4	20	22	12.2	0.41	Failure	Circular critical failure mechanism
146	20.39	11.15	11	16	45.8	0.2	Failure	Circular critical failure mechanism
147	19.03	3.9	28	35	21	0.11	Failure	Circular critical failure mechanism
148	17.98	1.65	30	20	8	0.3	Stable	Circular critical failure mechanism
149	20.96	6.65	40	40	12	0	Stable	Circular critical failure mechanism
150	20.96	11.65	28	40	12	0.5	Stable	Circular critical failure mechanism
151	19.97	3.35	29	34	6	0.3	Stable	Circular critical failure mechanism
152	18.77	10	10	25	50	0.1	Stable	Circular critical failure mechanism
153	18.77	10	20	30	50	0.1	Stable	Circular critical failure mechanism
154	18.77	8.35	20	30	50	0.2	Failure	Circular critical failure mechanism
155	20.56	5.4	27	30	40	0	Failure	Circular critical failure mechanism
156	16.47	3.85	0	30	3.6	0	Failure	Circular critical failure mechanism
157	18.8	4.8	25	20	30.6	0	Stable	Circular critical failure mechanism
158	18.8	19.15	20	20	30.6	0	Stable	Circular critical failure mechanism
159	28.4	13.05	38	35	100	0	Stable	Circular critical failure mechanism

Table 3 (continued)

NO	r (kN/m^3)	C (kPa)	φ (°)	β (°)	H (m)	r_u	Status	Location
160	24.96	40	45	53	120	0	Stable	Circular critical failure mechanism
161	18.46	4	0	30	6	0	Failure	Circular critical failure mechanism
162	22.38	3.35	35	30	10	0	Stable	Circular critical failure mechanism
163	21.98	6.65	36	45	50	0	Failure	Circular critical failure mechanism
164	18.8	5.1	30	25	10.6	0.38	Stable	Circular critical failure mechanism
165	18.8	4.8	25	31	76.8	0.38	Failure	Circular critical failure mechanism
166	21.47	2.3	30	30	88	0.45	Failure	Circular critical failure mechanism
167	13.97	4	26	45	20	0.12	Failure	Circular critical failure mechanism
168	17.98	8	30	45	15	0.25	Failure	Circular critical failure mechanism
169	22.38	33.3	45	45	10	0.4	Stable	Circular critical failure mechanism
170	22.38	3.35	35	45	50	0.25	Failure	Circular critical failure mechanism
171	19.97	6.65	36	45	50	0.25	Failure	Circular critical failure mechanism
172	19.97	6.65	36	45	50	0.5	Failure	Circular critical failure mechanism
173	20.96	15	25	49	12	0.3	Stable	Circular critical failure mechanism
174	20.96	10	35	40	12	0.4	Stable	Circular critical failure mechanism
175	19.97	13.35	30	30	15	0.3	Stable	Circular critical failure mechanism
176	17.98	15	25	25	14	0.3	Stable	Circular critical failure mechanism
177	18.97	10	35	35	11	0.2	Stable	Circular critical failure mechanism
178	19.97	13.35	40	40	10	0.2	Stable	Circular critical failure mechanism
179	18.83	8.25	21	21	37	0.5	Stable	Circular critical failure mechanism
180	18.83	3.45	21	34	37	0.3	Failure	Circular critical failure mechanism
181	18.77	8.35	10	25	50	0.2	Failure	Circular critical failure mechanism
182	18.77	6.65	10	25	50	0.3	Failure	Circular critical failure mechanism
183	19.08	3.35	10	25	50	0.4	Failure	Circular critical failure mechanism
184	18.77	6.65	20	30	50	0.3	Failure	Circular critical failure mechanism
185	19.08	3.35	20	30	50	0.4	Failure	Circular critical failure mechanism
186	21.98	6.65	22	20	180	0	Failure	Circular critical failure mechanism
187	21.98	6.65	22	20	180	0.1	Failure	Circular critical failure mechanism
188	22	10	35	45	10	0.403	Failure	Left bank accumulation body of Xiaodongjiang hydropower station, China
189	20	20	36	45	30	0.503	Failure	Longxi landslide of Longyangxia hydropower station, China
190	20	0.1	36	45	50	0.29	Failure	Chana landslide of Longyangxia hydropower station, China
191	20	0.1	36	45	50	0.503	Failure	Canal slope of Baoji gorge with Wei River diversion project, China
192	22	0	40	33	8	0.393	Stable	Yellowstone landslide in the Three Gorges of the Yangtze River, China
193	24	0	40	33	8	0.303	Stable	Baiyian landslide in the Three Gorges reservoir area, China
194	20	0	24.5	20	8	0.35	Stable	Baihuanping landslide in the Three Gorges reservoir area, China
195	18	0	30	33	8	0.303	Stable	Gaojiazui landslide in the Three Gorges reservoir area, China
196	27	43	35	43	420	0.29	Failure	Songshan ancient landslide at Lechangxia hydropower station, China
197	27	50	40	42	407	0.29	Stable	Back channel landslide in the Three Gorges reservoir area, China
198	27	35	35	42	359	0.29	Stable	Jipazi landslide in the Three Gorges reservoir area, China
199	27	37.5	35	37.8	320	0.29	Stable	Jiuxianping Landslide in the Three Gorges reservoir area, China
200	27	32	33	42.6	301	0.29	Failure	Heishe landslide, China
201	27	32	33	42.2	239	0.29	Stable	Liujiawuchang landslide in the Three Gorges reservoir area, China
202	27.3	14	31	41	110	0.29	Stable	Majiaba landslide in the Three Gorges Reservoir Area, China
203	27.3	31.5	29.703	41	135	0.293	Stable	Sandengzi landslide in the Three Gorges Reservoir Area, China
204	27.3	16.2	28	50	90.5	0.29	Stable	Yaqianwan landslide in the Three Gorges Reservoir Area, China
205	27.3	36	1	50	92	0.29	Stable	No.3 landslide of Sanbanxi hydropower station, China
206	27.3	10	39	41	511	0.29	Stable	Shijiapo landslide, China
207	27.3	10	39	40	470	0.29	Stable	Tanggudong landslide, China
208	25	46	35	47	443	0.29	Stable	Tianbao landslide, China
209	25	46	35	44	435	0.29	Stable	Shipingtai landslide of Xiaoxi hydropower station, China
210	25	46	35	46	432	0.29	Stable	Dongyemiao landslide, China
211	26	150	45	30	230	0.29	Stable	Hongtupo landslide, China
212	18.5	25	0	30	6.003	0.29	Failure	Lianziya landslide in the Three Gorges reservoir area, China

Table 3 (continued)

NO	r (kN/m^3)	C (kPa)	φ (°)	β (°)	H (m)	r_u	Status	Location
213	18.5	12	0	30	6.003	0.29	Failure	No. 6 landslide of Jishixia hydropower station, China
214	22	10	35	30	10	0.29	Stable	No.7 landslide of Tianshengqiao second cascade hydropower station, China
215	21	10	30.343	30	30	0.29	Stable	Kualiangzi landslide, China
216	22	10	36	45	50	0.29	Failure	No.1 landslide of Jishixia hydropower station, China
217	22	20	36	45	30	0.29	Failure	Daxi landslide, China
218	12	0.03	30	35	4	0.29	Failure	Right Bank landslide of Zihong reservoir, China
219	12	0	30	45	8	0.29	Failure	Zhongyangcun landslide, China
220	12	0	30	35	4	0.29	Stable	Zhaojiatang landslide, China
221	31.3	68	37	49	200.5	0.29	Failure	Yangdagou landslide of Xunyang hydropower station, China
222	20	30	36	45	50	0.29	Failure	Sujiaping Landslide, China
223	19.6	21.8	29.5	37.8	40.3	0.25	Stable	Maidipo Landslide, China
224	23.1	25.2	29.2	36.5	61.9	0.4	Stable	Maoping Landslide, China
225	23.8	31	38.7	47.5	23.5	0.31	Stable	Shaling Landslide, China
226	22.3	20.1	31	40.2	88	0.19	Stable	Niugunhan Landslide, China
227	23.5	25	20	49.1	115	0.41	Stable	Xieliupo Landslide, China
228	23	20	20.3	46.2	40.3	0.25	Stable	Zhaojiatang Landslide, China
229	21.5	15	29	41.5	123.6	0.36	Stable	Touzhaigou Landslide, China
230	23.4	15	38.5	30.3	45.2	0.28	Failure	Shenzhen reservoir diversion tunnel landslide, China
231	19.6	17.8	29.2	46.8	201.2	0.37	Stable	Taipingyi hydropower station diversion tunnel landslide, China
232	22.1	45.8	49.5	45.8	49.5	0.21	Stable	Bawangshan Landslide, China
233	18.82	25	14.6	20.32	50	0.4	Failure	Jiangxi Qiyi Reservoir, China
234	20	20	36	45	50	0	Failure	Unknown
235	27	40	35	47.1	292	0	Failure	Unknown
236	25	46	35	50	284	0	Stable	Unknown
237	31.3	68	37	46	366	0	Failure	Unknown
238	25	46	36	44.5	299	0	Stable	Unknown
239	27.3	10	39	40	480	0	Stable	Unknown
240	25	46	35	46	393	0	Stable	Unknown
241	25	48	40	49	330	0	Stable	Unknown
242	31.3	68.6	37	47	305	0	Failure	Unknown
243	25	55	36	45.5	299	0	Stable	Unknown
244	31.3	68	37	47	213	0	Failure	Unknown
245	26.49	150	33	45	73	0.15	Stable	Three Gorges hydropower project, China
246	26.7	150	33	50	130	0.25	Stable	Three Gorges hydropower project, China
247	26.89	150	33	52	120	0.25	Stable	Three Gorges hydropower project, China
248	26.57	300	38.7	45.3	80	0.15	Failure	Three Gorges hydropower project, China
249	26.78	300	38.7	54	155	0.25	Failure	Three Gorges hydropower project, China
250	26.81	200	35	58	138	0.25	Stable	Three Gorges hydropower project, China
251	26.43	50	26.6	40	92.2	0.15	Stable	Three Gorges hydropower project, China
252	26.69	50	26.6	50	170	0.25	Stable	Three Gorges hydropower project, China
253	26.81	60	28.8	59	108	0.25	Stable	Three Gorges hydropower project, China
254	27.8	27.8	27	41	236	0.1	Stable	Dingjiahe phosphorus mine, China
255	27.1	22	18.6	25.6	100	0.19	Failure	Guilin-Liuzhou highway, China
256	21.2	0	35	23.75	150	0.25	Failure	Xiaolangdi reservoir, China
257	21.2	0	35	23.75	150	0.25	Failure	Xiaolangdi reservoir, China
258	21.2	0	35	23.75	150	0.25	Stable	Xiaolangdi reservoir, China
259	21.2	0	35	23.75	150	0.25	Stable	Xiaolangdi reservoir, China
260	22.3	0	40	26.5	78	0.25	Stable	Xiaolangdi reservoir, China
261	18.6	0	32	26.5	46	0.25	Stable	Jingzhumiao reservoir, China
262	18.6	0	32	21.8	46	0.25	Stable	Jingzhumiao reservoir, China
263	18.8	9.8	21	19.29	39	0.25	Failure	Yuecheng reservoir, China
264	21.2	0	35	18.43	73	0.25	Stable	Yuecheng reservoir, China
265	17.2	10	24.25	17.07	38	0.4	Stable	Gushan reservoir, China

Table 3 (continued)

NO	r (kN/m^3)	C (kPa)	φ (°)	β (°)	H (m)	r_u	Status	Location
266	19	11.9	20.4	21.04	54	0.75	Stable	Laobu reservoir, China
267	18	5	26.5	15.52	53	0.4	Failure	Wenyuhe reservoir, China
268	18	5	22	15.52	53	0.4	Failure	Wenyuhe reservoir, China
269	17.4	20	24	18.43	51	0.4	Failure	Hongwuyi reservoir, China
270	17.8	21.2	13.92	18.43	51	0.4	Stable	Hongwuyi reservoir, China
271	18.8	8	26	21.8	40	0.4	Failure	Lingli reservoir, China
272	18.8	8	26	21.8	40	0.4	Failure	Lingli reservoir, China
273	18	21	21.33	21.8	40	0.4	Failure	Lingli reservoir, China
274	17.6	10	16	21.8	9	0.4	Stable	Zhejiang sea wall, China
275	17.6	10	8	21.8	9	0.4	Stable	Zhejiang sea wall, China
276	17.4	14.95	21.2	45	15	0.4	Failure	Hunan anxiang reservoir, China
277	27	27.3	29.1	21	565	0.26	Failure	Guzhang gaofeng slope, China
278	27	27.3	29.1	35	150	0.22	Failure	Guzhang gaofeng slope, China
279	27	27.3	29.1	37	184	0.3	Failure	Guzhang gaofeng slope, China
280	25	46	35	50	285	0.25	Stable	Chengmenshan open pit copper mine, China
281	20.45	16	15	30	36	0.25	Stable	Baijiagou earth slope, China
282	27	70	22.8	45	60	0.32	Stable	Jingping first stage hydropower station, China
283	22.4	10	35	45	10	0.4	Failure	Rockfill slope
284	20	20	36	45	50	0.5	Failure	Rockfill slope
285	20	0	36	45	50	0.25	Failure	Rockfill slope
286	20	0	36	45	50	0.5	Failure	Rockfill slope
287	22	0	40	33	8	0.35	Failure	Rockfill slope
288	24	0	40	33	8	0.3	Failure	Rockfill slope
289	20	0	24.5	20	8	0.35	Stable	Rockfill slope
290	18	5	30	20	8	0.3	Stable	Rockfill slope
291	27	40	35	43	420	0.25	Failure	Rockfill slope
292	27	50	40	42	407	0.25	Stable	Rockfill slope
293	27	35	35	42	359	0.25	Stable	Rockfill slope
294	27	37.5	35	37.8	320	0.25	Stable	Rockfill slope
295	27	32	33	42.6	301	0.25	Failure	Rockfill slope
296	27	32	33	42.4	289	0.25	Stable	Rockfill slope
297	27.3	14	31	41	110	0.25	Stable	Rockfill slope
298	27.3	31.5	29.7	41	135	0.25	Stable	Rockfill slope
299	27.3	16.8	28	50	90.5	0.25	Stable	Rockfill slope
300	27.3	26	31	50	92	0.25	Stable	Rockfill slope
301	27.3	10	39	41	511	0.25	Stable	Rockfill slope
302	27.3	10	39	40	470	0.25	Stable	Rockfill slope
303	25	46	35	47	443	0.25	Stable	Rockfill slope
304	25	46	35	44	435	0.25	Stable	Rockfill slope
305	25	46	35	46	432	0.25	Stable	Rockfill slope
306	26	150	45	30	200	0.25	Stable	Rockfill slope
307	18.5	25	0	30	6	0.25	Failure	Rockfill slope
308	18.5	12	0	30	6	0.25	Failure	Rockfill slope
309	22.4	10	35	30	10	0.25	Stable	Rockfill slope
310	21.4	10	30.34	30	20	0.25	Stable	Rockfill slope
311	25	46	35	46	393	0.25	Stable	Rockfill slope
312	25	48	40	49	330	0.25	Stable	Rockfill slope
313	31.3	68.6	37	47	305	0.25	Failure	Rockfill slope
314	25	55	36	45.5	299	0.25	Stable	Rockfill slope
315	31.3	68	37	47	213	0.25	Failure	Rockfill slope
316	0.657	0.176	0.333	0.66	0.041	0	Failure	Unknown
317	1	0.196	0.778	0.66	0.5	0	Stable	Unknown
318	0.914	1	1	0.943	1	0	Stable	Unknown

Table 3 (continued)

NO	r (kN/m^3)	C (kPa)	φ (°)	β (°)	H (m)	r_u	Status	Location
319	0.65	0.167	0	0.566	0.03	0	Failure	Unknown
320	0.752	0.067	0.674	0.566	0.1	0	Stable	Unknown
321	0.563	0.467	0.444	0.755	0.575	0	Failure	Unknown
322	0.718	0.166	0.289	0.415	0.053	0.7	Stable	Unknown
323	0.69	0.08	0.444	0.415	0.061	0.81	Failure	Unknown
324	0.767	0.057	0.711	0.528	0.064	0.98	Failure	Unknown
325	0.718	0.223	0.244	0.302	0.229	0.4	Failure	Unknown
326	0.67	0.078	0.622	0.66	0.105	0.22	Failure	Unknown
327	0.633	0.033	0.667	0.377	0.04	0.6	Stable	Unknown
328	0.738	0.133	0.889	0.755	0.06	0	Stable	Unknown
329	0.738	0.233	0.622	0.755	0.06	1	Stable	Unknown
330	0.703	0.067	0.644	0.642	0.03	0.6	Stable	Unknown
331	0.661	0.2	0.222	0.472	0.25	0.2	Stable	Unknown
332	0.661	0.2	0.444	0.566	0.25	0.2	Stable	Unknown
333	0.661	0.167	0.444	0.566	0.25	0.4	Failure	Unknown
334	0.724	0.108	0.589	0.566	0.2	0	Failure	Unknown
335	0.58	0.077	0	0.566	0.018	0	Failure	Unknown
336	0.662	0.096	0.556	0.377	0.153	0	Stable	Unknown
337	0.662	0.383	0.444	0.377	0.153	0	Stable	Unknown
338	1	0.261	0.844	0.66	0.5	0	Stable	Unknown
339	0.492	0.08	0.578	0.566	0.44	0	Failure	Unknown
340	0.879	0.8	1	1	0.6	0	Stable	Unknown
341	0.65	0.08	0	0.566	0.03	0	Failure	Unknown
342	0.788	0.067	0.778	0.566	0.05	0	Stable	Unknown
343	0.774	0.133	0.8	0.849	0.25	0	Failure	Unknown
344	0.662	0.102	0.667	0.472	0.053	0.76	Stable	Unknown
345	0.662	0.096	0.556	0.377	0.153	0.9	Failure	Unknown
346	0.756	0.046	0.667	0.585	0.384	0.76	Failure	Unknown
347	0.492	0.08	0.578	0.566	0.44	0.9	Failure	Unknown
348	0.633	0.16	0.67	0.849	0.1	0.24	Failure	Unknown
349	0.788	0.666	1	0.849	0.075	0.5	Stable	Unknown
350	0.788	0.067	0.778	0.849	0.05	0.8	Failure	Unknown
351	0.703	0.133	0.8	0.849	0.25	0.5	Failure	Unknown
352	0.703	0.133	0.8	0.849	0.25	1	Failure	Unknown
353	0.738	0.3	0.556	0.925	0.06	0.6	Stable	Unknown
354	0.738	0.2	0.778	0.755	0.06	0.8	Stable	Unknown
355	0.703	0.267	0.667	0.566	0.075	0.6	Stable	Unknown
356	0.633	0.3	0.556	0.472	0.07	0.6	Stable	Unknown
357	0.668	0.2	0.778	0.66	0.055	0.4	Stable	Unknown
358	0.703	0.267	0.889	0.755	0.05	0.4	Stable	Unknown
359	0.633	0.165	0.473	0.551	0.185	1	Failure	Unknown
360	0.633	0.069	0.473	0.642	0.185	0.6	Failure	Unknown
361	0.661	0.167	0.222	0.472	0.25	0.4	Failure	Unknown
362	0.661	0.133	0.222	0.472	0.25	0.6	Failure	Unknown
363	0.672	0.067	0.222	0.472	0.25	0.8	Failure	Unknown
364	0.661	0.133	0.444	0.566	0.25	0.6	Failure	Unknown
365	0.672	0.067	0.444	0.566	0.25	0.8	Failure	Unknown
366	0.774	0.133	0.489	0.377	0.9	0	Failure	Unknown
367	0.774	0.133	0.489	0.377	0.9	0.2	Failure	Unknown
368	17.6	39.5	30.2	50	38	0.04	Stable	Jorabat-Shillong expressway (NH-40)08 + 230
369	17.3	39	30	50	35	0.04	Stable	08 + 620
370	17.8	38.7	30.5	60	26	0	Stable	08 + 980
371	17.9	39	31.2	55	25	0.15	Stable	09 + 440

Table 3 (continued)

NO	r (kN/m^3)	C (kPa)	φ (°)	β (°)	H (m)	r_u	Status	Location
372	17.3	39	30	50	26	0.2	Stable	09 + 530
373	17.3	37.9	30	45	29	0.37	Stable	11 + 950
374	17.5	38.5	29	50	33	0.2	Stable	12 + 870
375	17.5	39.2	29.7	55	31	0	Stable	13 + 780
376	17.8	39.8	31.3	45	32	0.34	Stable	15 + 530
377	17.3	39	30	48	30	0.03	Stable	15 + 770
378	18.3	57.2	38.6	38	31	0.64	Stable	18 + 460
379	17.4	5	43.5	58	29	0.05	Failure	19 + 900
380	17.8	14	44.2	65	31	0.07	Failure	19 + 970
381	17.4	0	43.7	60	26	0.4	Failure	20 + 140
382	19.8	57.5	41.3	62	23	0.19	Stable	24 + 170
383	20.5	6.5	12.5	42	70	0	Failure	Yuan-Mo Highway
384	21.4	7.1	16.7	44	70	1	Failure	Yuan-Mo Highway
385	21.5	9.5	11.5	40	75	0	Failure	Yuan-Mo Highway
386	20.6	6.7	9.4	45	30	0	Failure	Yuan-Mo Highway
387	20.9	9.7	18.5	39	38	1	Failure	Yuan-Mo Highway
388	21.4	9.4	21.8	30	106	1	Failure	Yuan-Mo Highway
389	19.9	6.8	19.4	30	80	1	Failure	Yuan-Mo Highway
390	20.2	14.9	18.5	40	70	1	Failure	Yuan-Mo Highway
391	19	9	15.2	45	27	0	Failure	Yuan-Mo Highway
392	19.7	16.4	21.4	30	55	1	Failure	Yuan-Mo Highway
393	21.2	7.8	22.4	45	25	1	Failure	Yuan-Mo Highway
394	19.9	7.4	15.6	44	30	1	Failure	Yuan-Mo Highway
395	19.9	7.1	21.2	30	55	0	Failure	Yuan-Mo Highway
396	22.2	10.7	25.2	35	45	1	Failure	Yuan-Mo Highway
397	21.8	7.2	17.8	40	34	1	Failure	Yuan-Mo Highway
398	21.8	7.2	17.8	42	41	1	Failure	Yuan-Mo Highway
399	21.96	34.77	14.15	28	60	0	Stable	Yuan-Mo Highway
400	21.96	34.77	14.15	24	115	0	Stable	Yuan-Mo Highway
401	22.93	32.33	19.73	30	50	1	Stable	Yuan-Mo Highway
402	22.15	19.47	13.29	28	110	1	Stable	Yuan-Mo Highway
403	23.4	20	9	36.5	50	0	Stable	Yuan-Mo Highway
404	21.8	18.05	9.72	30	40	0	Failure	Yuan-Mo Highway
405	23.98	32.77	17.28	40	100	0	Failure	Yuan-Mo Highway
406	20.57	24.8	15.53	40	50	1	Stable	Yuan-Mo Highway
407	21.2	24.88	17.29	44	52	0	Failure	Yuan-Mo Highway
408	22.15	5	19	45	40	1	Failure	Yuan-Mo Highway
409	21.8	18.05	9.72	35	40	0	Failure	Yuan-Mo Highway
410	23.75	36.78	22.63	42	43	1	Failure	Yuan-Mo Highway
411	20.98	23.59	20	45	65	0	Failure	Yuan-Mo Highway
412	22.6	24.06	14.04	26	190	1	Stable	Yuan-Mo Highway
413	22.29	27.54	10.1	40	70	0	Stable	Yuan-Mo Highway
414	22.1	24.67	16.2	40	70	1	Stable	Yuan-Mo Highway
415	20.25	32.4	11.99	45	36	1	Failure	Yuan-Mo Highway
416	20.8	15.57	8.74	29.7	35	1	Failure	Yuan-Mo Highway
417	21.17	15.44	16	33	32	1	Failure	Yuan-Mo Highway
418	22.94	33.77	23.29	27	170	1	Stable	Yuan-Mo Highway
419	22.95	46.49	25.11	30	42	1	Stable	Yuan-Mo Highway
420	21.92	19.4	15.5	35	80	1	Failure	Yuan-Mo Highway
421	21.42	28.9	16.2	40	30	1	Stable	Yuan-Mo Highway
422	20.8	40.25	19.39	45	123	1	Failure	Yuan-Mo Highway
423	20.1	34.61	24.69	22	94	0	Stable	Yuan-Mo Highway
424	19.19	19.69	17.68	34	43	1	Failure	Yuan-Mo Highway

Table 3 (continued)

NO	r (kN/m^3)	C (kPa)	φ (°)	β (°)	H (m)	r_u	Status	Location
425	19.18	12.8	9.45	45	20	0	Failure	Yuan-Mo Highway
426	17.8	22.2	6.05	40	51.6	1	Failure	Yuan-Mo Highway
427	19.6	15.53	15.88	35	97	1	Failure	Yuan-Mo Highway
428	19.81	33.75	19.46	20	120	1	Stable	Yuan-Mo Highway
429	19.81	19.97	11.08	35	35	0	Failure	Yuan-Mo Highway
430	19.7	17	9.38	45	20	1	Failure	Yuan-Mo Highway
431	20.2	21.2	19.89	35	62	1	Failure	Yuan-Mo Highway
432	17.96	24.01	28	40	60	1	Failure	Yuan-Mo Highway
433	22	20	36	45	50	0	Failure	Unknown
434	22	0	36	45	50	0	Failure	Unknown
435	12	0	30	35	4	0	Stable	Unknown
436	12	0	30	45	8	0	Failure	Unknown
437	12	0	30	35	4	0	Stable	Unknown
438	31.3	68	37	49	200.5	0.25	Failure	Unknown
439	20	20	36	45	50	0.25	Failure	Unknown
440	27	40	35	47.1	292	0.25	Failure	Unknown
441	25	46	35	50	284	0.25	Stable	Unknown
442	31.3	68	37	46	366	0.25	Failure	Unknown
443	25	55	36	44.5	299	0.25	Stable	Unknown
444	27.3	10	39	40	480	0.25	Stable	Unknown

valuable tool for predicting slope stability, especially in cases that very easily fail and classes with very low stability followed by ET, RF, GBM and bagging models. However, the stacking model has a large number of calculations and long training time, so it is necessary to combine the super learner function in practical applications to improve the computational efficiency.

3. The importance scores of 0.2309, 0.2007 and 0.2003 obtained by the prediction variables more influence slope stability, of which are geotechnical material variables (γ, C and φ).
4. The relationship between slope stability and influencing factors is a high-dimensional complex nonlinear relationship, which is challenging to address by traditional modelling methods. The analysis of engineering examples shows that the ensemble learning algorithm can deal with this relationship well and achieve accurate and reliable prediction results, which has good applicability for slope stability evaluation. For future work, the introduction of samples and parameters that play an essential role can be added to develop an ensemble learning algorithm and improve its generalization and reliability, such as rainfall, earthquakes, human activities and other external or trigger factors.

Appendix

See Table 3.

Acknowledgements Supported by Open Research Fund of the State Key Laboratory of Geomechanics and Geotechnical Engineering, Institute of Rock and Soil Mechanics, and Chinese Academy of Sciences (Z019008), the Natural Science Foundation of China (Grant Nos. 42107214, 11972043 and 11902134)

References

1. Aljamaan H, Alazba A (2020) Software defect prediction using tree-based ensembles. In: Proceedings of the 16th ACM international conference on predictive models and data analytics in software engineering, pp 1–10
2. Anitescu C, Atroshchenko E, Alajlan N, Rabczuk T (2019) Artificial neural network methods for the solution of second-order boundary value problems. Comput Mater Contin 59(1):345–359
3. Bradley P (1997) The use of the area under the ROC curve in the evaluation of machine learning algorithms. Pattern Recogn 30(7):1145–1159
4. Breiman L (1996) Bagging predictors machine learning. Mach Learn 24:123–140
5. Chakraborty A, Goswami D (2017) Prediction of slope stability using multiple linear regression (MLR) and artificial neural network (ANN). Arab J Geosci 10(17):385
6. Chen L, Peng Z, Chen W, Peng W, Wu Q (2009) Artificial neural network simulation on prediction of clay slope stability based on fuzzy controller. J Cent South Univ (Sci Technol) 40(5):1381–1387

7. Chen C, Xiao Z, Zhang G (2011) Stability assessment model for epimetamorphic rock slopes based on adaptive neuro-fuzzy inference system. Electron J Geotech Eng 16:93–107
8. Cheng M, Hoang ND (2015) Typhoon-induced slope collapse assessment using a novel bee colony optimized support vector classifier. Nat Hazards 78(3):1961–1978
9. Dickson M, Perry GLW (2016) Identifying the controls on coastal cliff landslides using machine-learning approaches. Environ Model Softw 76:117–127
10. Dietterich TG (1997) Machine learning research: four current directions. AI Mag 18(4):97–136
11. Dietterich TG (2000) An experimental comparison of three methods for constructing ensembles of decision trees: bagging, boosting, and randomization. Mach Learn 40(2):139–157
12. Drucker H, Schapire R, Simard P (1993) Boosting performance in neural networks. Int J Pattern Recogn Artif Intell 7(04):705–719
13. Duncan JM (1996) State of the art: limit equilibrium and finite-element analysis of slopes. J Geotech Eng 123(7):577–596
14. Fattahi H (2017) Prediction of slope stability using adaptive neuro-fuzzy inference system based on clustering methods. J Min Environ 8(2):163–177
15. Feng X, Hudson J (2004) The ways ahead for rock engineering design methodologies. Int J Rock Mech Min Sci 41(2):255–273
16. Feng X, Wang Y, Lu S (1995) Neural network estimation of slope stability. J Eng Geol 3(4):54–61
17. Freund Y, Schapire RE (1997) A decision-theoretic generalization of on-line learning and an application to boosting. J Comput Syst Sci 55(1):119–139
18. Friedman JH (2001) Greedy function approximation: a gradient boosting machine. Ann Stat 29(5):1189–1232
19. Gounaridis D, Koukoulas S (2016) Urban land cover thematic disaggregation, employing datasets from multiple sources and RandomForests modeling. Int J Appl Earth Observ Geoinf 51:1–10
20. Griffiths D, Lane P (1999) Slope stability analysis by finite elements. Geotechnique 49(3):387–403
21. Gutta S, Wechsler H (1996) Face recognition using hybrid classifier systems. In: Proceedings of international conference on neural networks (ICNN'96). IEEE.
22. He F, Wu S, Zhang Y, Bao H (2004) A neural network method for analyzing compass slope stability of the highway. Acta Geosici Sin 25(1):95–98
23. Hoang ND, Pham AD (2016) Hybrid artificial intelligence approach based on metaheuristic and machine learning for slope stability assessment: a multinational data analysis. Expert Syst Appl 46:60–68
24. Hong H, Liu J, Bui D, Pradhan B, Acharya TD, Pham B, Zhu A, Chen W, Ahmad B (2018) Landslide susceptibility mapping using J48 Decision Tree with AdaBoost, Bagging and Rotation Forest ensembles in the Guangchang area (China). CATENA 163:399–413
25. Hosmer J, Lemeshow S, Sturdivant RX (2013) Applied logistic regression. Wiley, New York
26. Jin L, Feng W, Zhang J (2004) Maximum likelihood estimation on safety coefficiefficients of rocky slope near dam of Fengtan project. Chin J Rock Mech Eng 23(11):1891–1894
27. Kang F, Li J, Ma Z (2013) An artificial bee colony algorithm for locating the critical slip surface in slope stability analysis. Eng Optim 45(2):207–223
28. Kuhn M, Johnson K (2013) Applied predictive modeling. Springer, Berlin
29. Lee T, Lin H, Lu Y (2009) Assessment of highway slope failure using neural networks. J Zhejiang Univ 10(1):101–108
30. Li J, Wang F (2010) Study on the forecasting models of slope stability under data mining. In: Earth and space 2010: engineering, science, construction, and operations in challenging environments, pp 765–776
31. Li W, Yang S, Chen E, Qiao J, Dai L (2006) Neural network method of analysis of natural slope failure due to underground mining in mountainous areas. Yantu Lixue (Rock Soil Mech) 27(9):1563–1566
32. Lin H, Chang S, Wu J, Juang H (2009) Neural network-based model for assessing failure potential of highway slopes in the Alishan, Taiwan Area: pre-and post-earthquake investigation. Eng Geol 104(3–4):280–289
33. Lin S, Zheng H, Jiang W, Li W, Sun G (2020) Investigation of the excavation of stony soil slopes using the virtual element method. Eng Anal Bound Elem 121:76–90
34. Lin Y, Zhou K, Li J (2018) Prediction of slope stability using four supervised learning methods. IEEE Access 6:31169–31179
35. Liu Z, Shao J, Xu W, Chen H, Zhang Y (2014) An extreme learning machine approach for slope stability evaluation and prediction. Nat Hazards 73(2):787–804
36. Lu P, Rosenbaum M (2003) Artificial neural networks and grey systems for the prediction of slope stability. Nat Hazards 30(3):383–398
37. Manouchehrian A, Gholamnejad J, Sharifzadeh M (2014) Development of a model for analysis of slope stability for circular mode failure using genetic algorithm. Environ Earth Sci 71(3):1267–1277
38. Marjanović M, Kovačević M, Bajat B, Voženílek V (2011) Landslide susceptibility assessment using SVM machine learning algorithm. Eng Geol 123(3):225–234
39. Michalowski LR (1995) Slope stability analysis: a kinematical approach. Geotechnique 45(2):283–293
40. Pedregosa F, Varoquaux G, Gramfort A, Michel V, Thirion B (2011) Scikit-learn: machine learning in python. J Mach Learn Res 12:2825–2830
41. Qi C, Tang X (2018) A hybrid ensemble method for improved prediction of slope stability. Int J Numer Anal Methods Geomech 42(15):1823–1839
42. Qi C, Tang X (2018) Slope stability prediction using integrated metaheuristic and machine learning approaches: a comparative study. Comput Ind Eng 118:112–122
43. Sakellariou M, Ferentinou M (2005) A study of slope stability prediction using neural networks. Geotech Geol Eng 23(4):419–445
44. Samui P (2008) (2008) Slope stability analysis: a support vector machine approach. Environ Geol 56(2):255–267
45. Schapire RE, Singer Y (1999) Improved boosting algorithms using confidence-rated predictions. Mach Learn 37(3):297–336
46. Shimshoni Y, Intrator N (1998) Classification of seismic signals by integrating ensembles of neural networks. IEEE Trans Signal Process 46(5):1194–1201
47. Simm J, Abril I (2014) Extratrees: extremely randomized trees (ExtraTrees) method for classification and regression. R package version 1.0. 5.
48. Sun G, Lin S, Zheng H, Tan Y, Sui T (2020) The virtual element method strength reduction technique for the stability analysis of stony soil slopes. Comput Geotech 119:103349
49. Wang CH (2004) Study on prediction methods for high engineering slope. Master thesis
50. Wang L, Wu C, Tang L, Zhang W, Lacasse S, Liu H, Gao L (2020) Efficient reliability analysis of earth dam slope stability using extreme gradient boosting method. Acta Geotech 15(11):3135–3150
51. Wang H, Xu W, Xu R (2005) Slope stability evaluation using back propagation neural networks. Eng Geol 80(3–4):302–315
52. Wen S, La H, Wang C (2013) Analysis of influence factors of slope stability. Appl Mech Mater Trans Tech Publ 256:34–38

53. Wolpert DH (1992) Stacked generalization. Neural Netw 5(2):241–259
54. Xiao Z, Chen C, Ji Y (2011) Applying adaptive neuro-fuzzy inference system to stability assessment of reservoir slope. Bull Soil Water Conserv 31(5):186–190
55. Xu W, Shao J (1998) Artificial neural network analysis for the evaluation of slope stability. Application of numerical methods to geotechnical problems. Springer, Berlin, pp 665–672
56. Xu F, Xu W, Wang K (2009) Slope stability analysis using least square support vector machine optimized with ant colony algorithm. J Eng Geol 17(2):253–257
57. Yan X, Li X (2011) Bayes discriminant analysis method for predicting the stability of open pit slope. In: 2011 International conference on electric technology and civil engineering (ICETCE). IEEE, pp 147–150
58. Yun L, Keping Z, Jielin L (2018) Prediction of slope stability using four supervised learning methods. IEEE Access 6:31169–31179
59. Zhao H, Yin S, Ru Z (2012) Relevance vector machine applied to slope stability analysis. Int J Numer Anal Meth Geomech 36(5):643–652
60. Zheng F, Leung YF, Zhu J, Jiao Y (2019) Modified predictor-corrector solution approach for efficient discontinuous deformation analysis of jointed rock masses. Int J Numer Anal Meth Geomech 43(2):599–624
61. Zheng F, Zhuang X, Zheng H, Jiao Y, Timon R (2020) Kinetic analysis of polyhedral block system using an improved potential-based penalty function approach for explicit discontinuous deformation analysis. Appl Math Model 82:314–335
62. Zhou Z, Jiang Y, Yang Y, Chen S (2002) Lung cancer cell identification based on artificial neural network ensembles. Artif Intell Med 24(1):25–36
63. Zhou J, Li X, Mitri HS (2015) Comparative performance of six supervised learning methods for the development of models of hard rock pillar stability prediction. Nat Hazards 79(1):291–316
64. Zhou J, Li E, Yang S, Wang M, Mitri H (2019) Slope stability prediction for circular mode failure using gradient boosting machine approach based on an updated database of case histories. Saf Sci 118:505–518
65. Zhou S, Rabczuk T, Zhuang X (2018) Phase field modeling of quasi-static and dynamic crack propagation: COMSOL implementation and case studies. Adv Eng Softw 122:31–49
66. Zhou S, Zhuang X, Rabczuk T (2018) A phase-field modeling approach of fracture propagation in poroelastic media. Eng Geol 240:189–203
67. Zhou S, Zhuang X, Zhu H, Rabczuk T (2018) Phase field modeling of crack propagation, branching and coalescence in rocks. Theor Appl Fract Mech 96:174–192
68. Zhu C (2005) Analysis and evaluation of slope stability—taking yuanmo expressway slope as an example. Kunming University of Science and Technology
69. Zhu B, Zhou D, Chen S, Wang L (2011) Evaluation of slope stability by improved BP neural network with L-M method. West-China Explor Eng 10:21–24
70. Zhuang X, Zheng F, Zheng H, Jiao Y, Rabczuk T, Wriggers P (2021) A cover-based contact detection approach for irregular convex polygons in discontinuous deformation analysis. Int J Numer Anal Meth Geomech 45:208–233